C S P

The DOE Center of Excellence for the Synthesis and Processing of Advanced Materials

BASIC ENERGY SCIENCES
DIVISION OF MATERIALS SCIENCE
& ENGINEERING

Member Laboratories: Ames Laboratory, Argonne National Laboratory, Brookhaven National Laboratory, Idaho National Engineering and Environmental Laboratory, University of Illinois Frederick Seitz Materials Research Laboratory, Lawrence Berkeley National Laboratory, Lawrence Livermore National Laboratory, Los Alamos National Laboratory, National Renewable Energy Laboratory, Oak Ridge National Laboratory, Pacific Northwest National Laboratory, and Sandia National Laboratories

Research Briefs

For questions and additional information contact:

George A. Samara
Sandia National Laboratories/NM
Phone: (505) 844-6653
Fax: (505) 844-4045
E-mail: gasamar@sandia.gov

C S P

The DOE Center of Excellence for the
Synthesis and Processing
of Advanced Materials

BASIC ENERGY SCIENCES
DIVISION OF MATERIALS SCIENCE
& ENGINEERING

Research Briefs

August 2001

Table of Contents

Research Briefs

Table of Contents

Preface

This publication, *Research Briefs*, is designed to inform present and potential customers and partners of the DOE Center of Excellence for the Synthesis and Processing of Advanced Materials (CSP) about significant advances resulting from Center-coordinated research. The format for *Research Briefs* is an easy-to-read, not highly technical, concise presentation of the accomplishments. Each *Brief* provides a statement of the motivation for the research followed by a description of the accomplishment and its significance.

The Center is a distributed center for promoting coordinated, collaborative research partnerships related to the synthesis and processing of advanced materials. It was established by the Department of Energy's Division of Materials Sciences and Engineering, Office of Basic Energy Sciences and the DOE Laboratories in recognition of the enabling role of materials synthesis and processing to numerous materials fabrication- and manufacturing-intensive technologies. The participants include investigators from 12 DOE national laboratories, universities and the private sector. The Center has a technology perspective provided by a Technology Steering Group.

By bringing together synergistic activities and capabilities in selected focus areas of materials synthesis and processing, the Center's goal is to be a vehicle for providing added value and making impact. The Center is also allowing better coordinated strategic planning by the Division of Materials Sciences and Engineering and the Laboratories and faster response time to special needs and opportunities. Additionally, the Center is serving as a model of R and D integration within the Department of Energy as well as a model of cooperation among the participating institutions.

The overall objective of the Center is,
To enhance the science and engineering of materials synthesis and processing in order to meet the programmatic needs of the Department of Energy and to facilitate the technological exploitation of materials.

Synthesis and processing (S&P) are those essential elements of Materials Science and Engineering (MS&E) that deal with (1) the assembly of atoms or molecules to form materials, (2) the manipulation and control of the structure at all levels from the atomic to the macroscopic scale, and (3) the development of processes to produce materials for specific applications. Clearly, S&P represent a large area of MS&E that spans the range from fundamental research to technology. The goal of basic

research in this area ranges from the creation of new materials and the improvement of the properties of known materials, to the understanding of such phenomena as diffusion, crystal growth, sintering, phase transitions, to the development of novel diagnostic, modeling and processing approaches, etc. On the applied side, the goal of S&P is to translate scientific results into useful materials by developing processes capable of producing high quality cost-effective products.

The technical emphasis of the Center is on a number of focused multilaboratory projects which draw on the complementary strengths of the member institutions in their ongoing research programs. These projects were selected on the basis of the following criteria:

- scientific excellence
- clear relationship to energy technologies
- involvement of several laboratories
- existing or potential partnerships with DOE Technologies-funded programs
- existing or potential "in-kind" partnerships with industry

Each Project is coordinated by a knowledgeable representative from one of the participating laboratories. The Projects covered in this issue of *Research Briefs* and their Coordinators are listed in the accompanying table (p. 7). A few selected accomplishments from each of the Projects are presented. An Executive Summary provides highlights of these accomplishments organized by Project. Readers are encouraged to contact any of the Coordinators for information about the Center and its accomplishments.

Two of the projects listed in the table on page 7, namely, *Interfacial Adhesion Related to Protective Oxides Grown on Metallic Substrates* and *High Efficienty Photovoltaics* will graduate at the end of FY2001. Center Projects are graduated after achieving their objectives, but no later than five years after start. The two graduating Projects will be replaced by the following two projects: *Synthesis and Processing of Carbon-Based Nanostructured Materials* and *Granular Flow and Kinetics*. Future issues of *Research Briefs* will highlight some of the accomplishments of these two projects.

George A. Samara
August 2001

The Center's Member Laboratories

The member laboratories of the Center are:

- Ames Laboratory (Ames)
- Argonne National Laboratory (ANL)
- Brookhaven National Laboratory (BNL)
- Idaho National Engineering and Environmental Laboratory (INEEL)
- University of Illinois Frederick Seitz Materials Research Laboratory (UI/MRL)
- Lawrence Berkeley National Laboratory (LBNL)
- Lawrence Livermore National Laboratory (LLNL)
- Los Alamos National Laboratory (LANL)
- National Renewable Energy Laboratory (NREL)
- Oak Ridge National Laboratory (ORNL)
- Pacific Northwest National Laboratory (PNNL)
- Sandia National Laboratories (SNL)

Membership of the Technology Steering Group

Member	**Affiliation**
Prof. L. Eric Cross	Pennsylvania State University
Dr. David W. Johnson, Jr.	Agere Systems
Dr. Hylan B. Lyon	Marlow Industries
Dean Paul S. Peercy	University of Wisconsin
Dr. Charles Sorrell	DOE/Energy Efficiency & Renewable Energy
Dr. John Stringer	Electric Power Research Institute (EPRI)
Dr. Arthur Yang	Arthur Yang Industrial Science and Technology Network, Inc.

Center Projects Covered In This Issue Of *Research Briefs* and Their Coordinators

Project	Coordinator(s)
Isolated and Collective Phenomena in Nanocomposite Magnets	Samuel D. Bader (ANL) Phone: (630) 252-4960 E-mail: bader@anl.gov
Smart Materials Based on Electroactive Polymers	Gregory J. Exarhos (PNNL) Phone: (509) 375-2440 E-mail: greg.exarhos@pnl.gov
Design and Synthesis of Ultrahigh-Temperature Intermetallics	Roddie R. Judkins (ORNL) Phone: (865) 574-4572 E-mail: judkinsrr@ornl.gov and R. Bruce Thompson (Ames) Phone: (515) 294-8152 E-mail: thompsonrb@cnde.iastate.edu
Nanoscale Phenomena in Perovskite Thin Films	Orlando Auciello (ANL) Phone: (630) 252-1685 E-mail: auciello@anl.gov and Duane Dimos (SNL/NM) Phone: (505) 844-6385 E-mail: dbdimos@sandia.gov
The Science of Localized Corrosion	Kevin Zavadil (SNL/NM) Phone: (505) 845-8442 E-mail: krzavad@sandia.gov
Interfacial Adhesion Related to Protective Oxides Grown on Metallic Substrates	Linda L. Horton (ORNL) Phone: (865) 574-5081 E-mail: hortonll@ma160.ms.ornl.gov
High Efficiency Photovoltaics	Satyen Deb (NREL) Phone: (303) 384-6405 E-mail: satyen_deb@nrel.gov
Controlled Defect Structures in Rare-Earth-Ba-Cu-O Cuprate Superconductors	David O. Welch (BNL) Phone: (631) 344-3517 E-mail: dwelch@bnl.gov
Overall Center Coordinator	George A. Samara (SNL/NM) Phone: (505) 844-6653 E-mail: gasamar@sandia.gov

Executive Summary

The *Research Briefs* presented in this publication are intended to inform the Center's present and potential customers and partners about significant advances resulting from Center-coordinated research. Selected accomplishments from each of eight Center focused projects are presented. This Executive Summary states the overall objective of each project followed by highlights of the accomplishments presented later in more detail.

Isolated and Collective Phenomena in Nanocomposite Magnets

Objective

Develop improved understanding of magnetic properties and improved magnetic materials using nanoscale mixtures of hard magnets, soft magnets and non-magnetic materials.

Highlights

- The stability of exchange coupling (and thus the magnetization) to field cycling was investigated in a model (Sm-Co/Fe) exchange-spring magnet using hard/soft thin film structures. It is found that the stability is strongly influenced by the microstructure, crystal orientation and magnetic anisotropies in the plane of the film. A uniaxial microstructure of the hard phase is desired. (p. 14)

- Systematic tailoring of the microstructure has produced nanocomposite permanent magnets with the highest coercivity in the Fe-Nd-B system. The largest observed coercivity, H_c=2.75T is ~83% of the theoretical maximum for this system. (p. 16)

- Strong collective magnetism from dipolar interactions in dipolar nanocomposites consisting of superparamagnetic particles aligned into chains in a frozen matrix has been demonstrated. The strong susceptibility enhancement and low electrical conductivity of these composites are important for applications in high frequency transormers, sensors and memory storage. (p. 18)

.

Smart Materials Based on Electroactive Polymers

Objective

Develop a framework for the rational design of self-assembled nanostructured block copolymers that offer significant advantages over conventional materials for the active regulation of transport phenomena.

Highlights

- Oriented, conducting polymer nanofibers, nanowires and films with ordered nanoporosity over micrometer and larger length scales have been prepared electrochemically for the first time. The synthesis employs the structure-directing properties of templating phases bound to an electrode surface where the polymerization reaction occurs. (p. 20)

- A triblock copolymer that self-assembles into a lamellar phase has been driven to a number of other stable morphologies by the addition of another polymer. The resulting structure of the polymer-copolymer hybrid is stabilized by the resident polymer chemistry and the amount of polymer phase present. (p. 22)

- Two polymerization routes have been used to form self-assembled films of poly n-isopropyl acrylamide (PNIPAM) films on porous silica membranes for the reversible adsorption and release of proteins. Protein sticks to the PNIPAM when it is heated above 35° C, but it is rapidly released on cooling below this temperature. (p. 24)

Design and Synthesis of Ultrahigh-Temperature Intermetallics

Objective

Generate the knowledge required to establish a scientific basis for the design and processing of transition-metal silicides and materials based on silicides for structural applications at temperatures of 1400°C and above.

Highlights

- The substitution of niobium (Nb) or vanduim (V) for molybdenum (Mo) in Mo_5Si_3 greatly reduces the coefficient of thermal expansion (CTE) anisotropy between the *c*- and *a*-axes of Mo_5Si_3 in agreement with *ab initio* theoretical calculations. The CTE ratio, CTE(*c*)/CTE(*a*) is reduced from 2 for Mo_5Si_3 to 1.5 for both Mo_4NbSi_3 and Mo_4VSi_3. (p. 26)

- It has been shown that the boron-modified molybdenum silicide alloy, Mo-12Si-8.5B (at.%), can be processed to be considerably tougher and more fatigue resistant than both monolithic $MoSi_2$ and Nb-sphere reinforced $MoSi_2$. Additionally, the crack-growth resistance of this B-modified alloy increases progressively with increasing temperature up to 1300°C. (p.28)

- A process to improve the fracture toughness of Mo-Si-B alloys has been developed and demonstrated for a Mo-20Si-10B (at.%) alloy. The process is based on the consolidation of Mo-coated Mo-Si-B particles leading to the formation of Mo_3Si and Mo_5SiB_2 phases in a continuous α-Mo matrix. (p. 30)

Nanoscale Phenomena in Perovskite Thin Films

Objective

Develop the scientific basis for controlling nucleation, growth and strain in ferroelectric perovskite thin films.

Highlights

- The ferroelectric properties of $KTaO_3/KNbO_3$ superlattices were determined by atomic level simulations. The insights obtained are crucial to understanding the properties of Ferroelectric-Paraelectric heterostructures. (p. 32)
- The effects of lanthanide dopants on the atomic structure and macroscopic properties of PZT films were investigated. The polarization and fatigue performance of the amphoteric dopant Dy are substantially better than the similarly-prepared, industry standard La-doped film. (p. 34)
- The use of conductive amorphous Ti-Al film as a diffusion barrier on Si during oxidation (20 - 700°C) was investigated using atomic-level, surface diagnostic techniques. The a-Ti/Al is found to be stable to 600°C in oxygen, making it a viable candidate for the integration of ferroelectric capacitors with Si devices (p. 36).

The Science of Localized Corrosion

Objective

Advance the fundamental understanding of the mechanisms leading to the initiation, propagation and cessation of localized corrosion of aluminum and its alloys to permit accurate life predictions and intelligent designs.

Highlights

- A model of pit interactions in the localized corrosion of Al that allows simulation of experimental results was developed. Important input parameters include pit corrosion rates, local pHs, pit stability pHs, and pit separation distance. The results reveal the long-range effects of chemical interactions in pitting. (p. 38)
- A microelectrochemical cell has been used to measure the electrochemical characteristics of the Al matrix as well as those of intermetallic particles dispersed in 2024 - T_3 aluminum alloy. The pitting potential of the alloy coincides with the breakdown potential of the intermetallics (and both are much lower than for the particle-free Al matrix) suggesting that the two processes are closely related. (p. 40)
- Scanning electrochemical microscopy was developed to image the local electrochemical activity at Al electrodes. The results are the first to show a direct link between sites of oxide breakdown and local electrical conductivity in the Al system. (p. 42)

Interfacial Adhesion Related to Protective Oxides Grown on Metallic Substrates

Objective

Further the fundamental understanding of the interfacial bonding and dynamics that underlie oxide-metal adhesion and the energetics associated with decohesion for systems relying on protective alumina through theoretical calculations, experimentation and modeling.

Highlights

- Micro x-ray photoelectron spectroscopy studies have identified the segregants and their chemical state at the alloy/Al_2O_3 interface for two different iron-based high temperature alloys. While both alloys form the same oxide film, the nature of the interfacial segregants are substantially different. (p. 44)

- Synchrotron x-ray measurements were used for rapid determination of strain in thin chromia films formed by the high temperature oxidation of an Fe-Ni-Cr alloy. Large strains can lead to decohesion at the metal/oxide interface. (p. 46)

- Finite element continuum models were developed to analyze surface and interface cracking of protective oxides at regions of local curvature (e.g., corners) during cooling from high temperature. The results have led to an improved understanding of failure mechanisms and local fracture behavior. (p. 48)

High Efficiency Photovoltaics

Objective

Generate advances in scientific understanding that will impact the efficiency, cost and reliability of thin film photovoltaics cells by addressing short-and long-term basic research issues.

Highlights

- The origin of the relatively low electron lifetime, mobility and diffusion length in GaAsN and GaInAsN has been investigated using a variety of experimental techniques. The results suggest a model whereby these materials are viewed as heavily doped semiconductors such as GaAs:Si and not as alloys. Nitrogen forms impurity bands from interactions between the isoelectronic impurity levels (the NN traps) leading to the above degradation in properties compared to GaAs. (p. 50)

- Hot-Wire Chemical Vapor Deposition (HWCVD) combined with post-deposition metal-induced crystallization has been shown to produce Si films with 0.1 μm grains suggesting that this approach may be viable for producing thin Si film solar cells. The fast growth rates and low-temperature processing involved are attractive aspects of this approach. (p. 52)

- A resonance acoustic technique has been developed that has the potential for providing on-line quality control of Si wafers at different processing steps. In this technique, the width of the resonance frequency peak provides a measure of the stress buildup in the wafer. (p. 54)

Controlled Defect Structures in Rare-Earth-Ba-Cu-O Cuprate Superconductors

Objective

Provide an integrated scientific understanding of lattice defects and their nanoscale structure in the "123" rare-earth cuprates and related compounds, their dependence on the various methods of synthesis, and their relationship to the resulting superconducting properties.

Highlights

- Reaction kinetics and transmission electron microscopy studies have led to an understanding of the mechanism for the growth of *a-b* textured, *c*-axis YBCO thick films using the BaF_2 post-deposition reaction process. Thick films are needed for carrying large currents in electric power applications. (p. 56)

- It was discovered that Sr doping of grain boundaries in $YBa_2Cu_3O_{7-\delta}$ (YBCO) improves the critical current density (J_c) by a factor of 3 to 5 without any reduction in the superconducting transition temperature. This improvement is attributed to the reduction in tensile strain associated with the incorporation of dopant atoms in the dislocation cores of grain boundaries. (p. 58)

- High critical current density (J_c) in zero magnetic field was demonstrated for thick (3μm) $HgBa_2Ca_1Cu_2O_x$ (Hg-1212) superconducting films with T_c=124K deposited on model substrates. While J_c of the as-grown films decreases rapidly with applied field (H), we have also found that the introduction of columnar defects by heavy-ion irradiation dramatically improves J_c (H). (p. 60)

Research Briefs

Stability of Exchange-Spring Permanent Magnets

J. S. Jiang *and* ***S. D. Bader***
Argonne National Laboratory

Motivation—Exchange spring permanent magnets consist of a nanodispersion of interfacial exchange coupled hard and soft magnetic phases that combine the high magnetization of the soft phase with the high anisotropy of the hard phase to attain a high energy product. In a dynamic application the magnet might experience a strong demagnetizing field that could cause a catastrophic collapse of the magnetic induction. Thus the stability of the magnet to field cycling is a critical issue. The robustness of interfacial exchange coupling will undoubtedly affect the viability of exchange-spring magnets in various device and materials engineering schemes.

Accomplishment—We have systematically investigated the stability of exchange coupling in model exchange-spring magnets using hard/soft thin film structures. Epitaxial thin film growth allows the magnetic properties to be tailored by controlling the microstructure, crystal orientation and magnetic anisotropies in the plane of the film. Samples of Sm-Co/Fe bilayer structures (schematically illustrated in Fig. 1) were grown onto single-crystal MgO(110) and (100) and quartz substrates to create Sm-Co hard layers with uniaxial, biaxial and random in-plane anisotropies, respectively.

The magnetic stability of Sm-Co/Fe bilayers was studied by switching the magnetization of the Fe layer multiple times in a reverse field. The hard/soft exchange coupling was monitored using the magneto-optic Kerr effect (MOKE) as the Fe magnetization was reversed in the applied field for as many as 10^7 times.

Figure 2 shows the change in the exchange coupling field (H_{ex}) with the number of field cycles for the three different kinds of samples. The uniaxial exchange-spring bilayer shows a rapid initial decay in H_{ex} and then a plateau. However, the biaxial and the in-plane random bilayers show a much slower decay in H_{ex} that does not stabilize even after 10^7 field cycles. The different decay behaviors in the uniaxial and biaxial samples are attributed to the different microstructures and spin configurations at the interfacial pinning layers. High-resolution electron microscopy (with our collaborator K. Krishnan, LBNL) reveals this. The biaxial Sm-Co has a twinned bicrystalline structure with small grains whose easy axes are either parallel or perpendicular to each other, whereas the uniaxial Sm-Co contain stacking faults that are normal to the easy axis, due to intergrowths of different Sm-Co alloy polytypoids. In the uniaxial Sm-Co, the planar stacking faults provide effective domain-wall pinning which prevents further propagation of reversed domains. However, the magnetization of some of the grains in the biaxial and in-plane random Sm-Co slowly relax into their local preferred directions with field cycling.

Significance—High-performance permanent magnets may afford the advantages of increased efficiency in energy production and energy systems. Understanding the microstructure-properties relationships is necessary in order to optimize exchange-spring permanent magnets. Our study shows that for applications of exchange - spring magnets that require long-term stability, the uniaxial microstructure of the hard phase is preferred.

Contact: S. D. Bader, Argonne National Laboratory
Phone: (630) 252-4960, Fax: (630) 252-9595, E-mail: bader@anl.gov

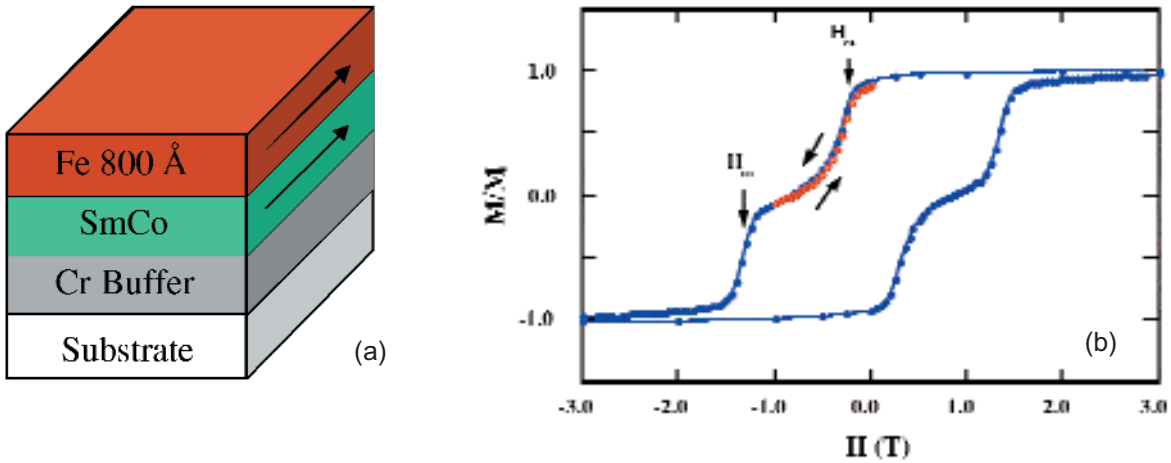

Figure 1. (a) Schematic illustration of a Fe/Sm-Co bilayer structure. (b) Low-temperature hysteresis loop (solid symbols) for a Fe/Sm-Co bilayer. The open symbols define the recoil curve showing the "exchange-spring" behavior. The Fe magnetization starts to reverse at H_{ex} but is pinned at the interface by the underlying Sm-Co layer and is fully reversible before the Sm-Co layer switches at H_{irr}.

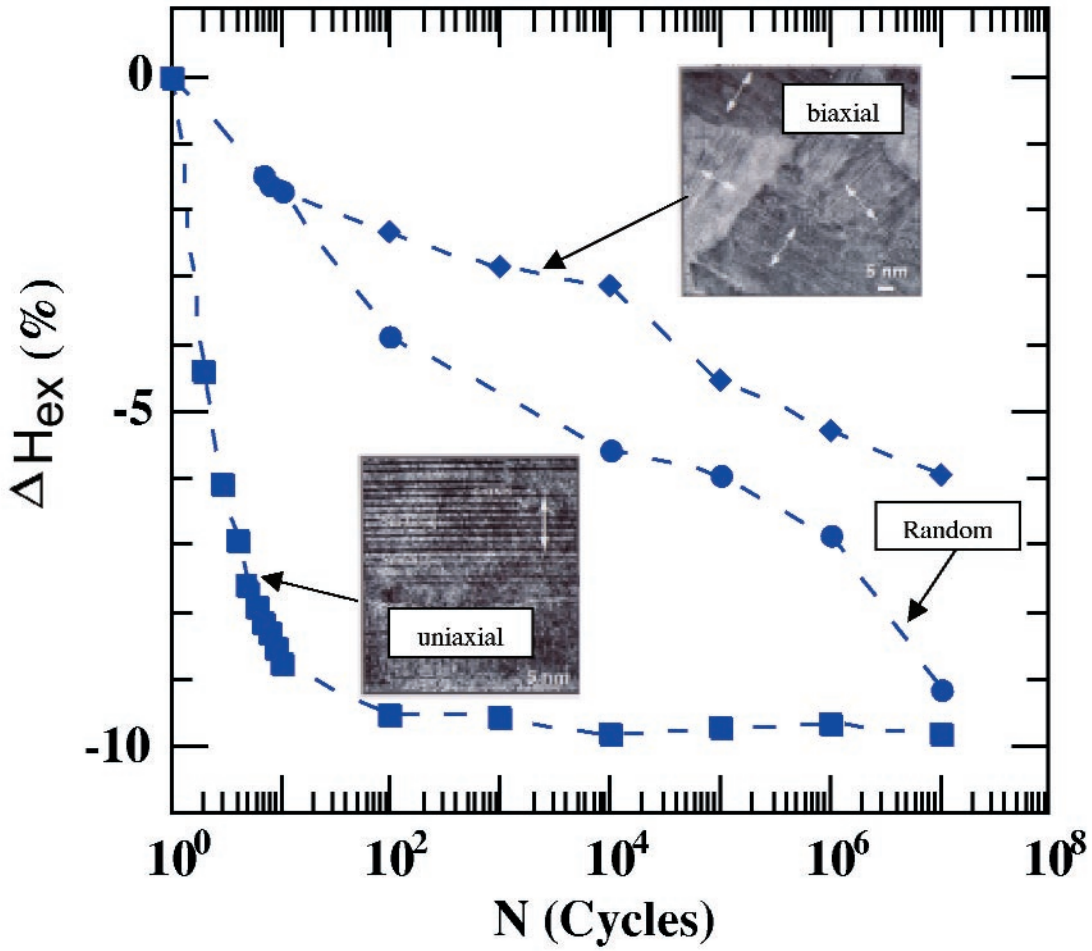

Figure 2. The change in exchange coupling field ΔH_{ex} ($\Delta H_{ex} = (H_{ex} - H_{ex0})/H_{ex0}$, where H_{ex0} is that of the first loop) measured at room temperature as a function of the number of field cycles N for Sm-Co(80 nm)/Fe(80 nm) exchange spring bilayers with uniaxial, biaxial and random in-plane SmCo layer. The insets are high-resolution electron micrographs of Sm-Co showing the different microstructures. The white arrows indicate the easy axes.

Coercivity Limits and Mechanisms in Nd-Fe-B Nanocomposite Magnets

Kannan M. Krishnan, Er. Girt *and* ***G. Thomas***
Lawrence Berkeley National Laboratory

Motivation—Performance of permanent magnets for a variety of applications is often determined by the maximum energy product $(BH)_{max}$. In order to obtain high $(BH)_{max}$ permanent magnetic materials have to have large coercivity. In theory the coercive field of ideally oriented, non-interacting, single domain, magnetic particles, assuming K_1 is much bigger than K_2, was shown to be $H_c = 2K_1/M_s - N M_s$, where K_1 and K_2 are the magnetocrystalline anisotropy constants, M_s is the spontaneous magnetization and N is the demagnetization factor. For randomly oriented non-interacting particles, the Stoner-Wohlfarth model predicts that the value of H_c decreases to about half. However, experimentally obtained values of H_c in permanent magnets are 3 to 10 and 2 times smaller for well oriented and randomly oriented samples, respectively. This discrepancy was attributed to inter-particle interaction and the microstructure of the permanent magnets. In order to understand the difference between the theoretically predicted and experimentally obtained results for H_c we prepared rapidly quenched, Nd-rich, $Nd_xFe_{14}B$ ($2<x<150$) ribbons. By changing the amount of the non-magnetic Nd matrix the strength between $Nd_2Fe_{14}B$ particles was tailored ranging from strongly magnetically interacting particles in pure $Nd_2Fe_{14}B$ to nearly non-interacting $Nd_2Fe_{14}B$ particles in $Nd_{150}Fe_{14}B$. The latter is expected to approach the high coercive field predicted by the Stoner-Wohlfarth model.

Accomplishment—The largest coercivity in the Nd-Fe-B system was achieved by systematically tailoring the microstructure from strongly interacting $Nd_2Fe_{14}B$ grains to magnetically isolated $Nd_2Fe_{14}B$ grains in a Nd-rich matrix (fig 1a). The crystal structure, phase purity and magnetic properties of the Nd-Fe-B samples were extensively measured. In particular, energy-filtered imaging (fig 1d), using spatially resolved measurements of inner-shell ionization edges (fig 1c), was critical in evaluating the particle shapes (platelets with the crystallographic c-axis normal to the plate), size (~ 100 x 40 x 25 nm) and distribution (fig 1b). For randomly oriented, non-interacting particles, the largest observed coercivity, H_c ~ 2.75 T (fig 1e) is ~ 83% of the theoretical limit expected for Stoner-Wohlfarth coherent rotation behavior (fig 1f). Initial magnetization curves of thermally demagnetized Nd-Fe-B samples show a systematic increase in susceptibility with an increase in Nd concentration as a result of a competition between contributions from strongly-interacting $Nd_2Fe_{14}B$ grains with grain sizes smaller or equal to the magnetic domain size and completely isolated multidomain $Nd_2Fe_{14}B$ grains. The focus of current work is to further understand the coercivity mechanism in such nanocomposite magnets.

Significance—Systematic tailoring of the microstructure has produced nano-composite permanent magnets with the highest coercivity in the Fe-Nd-B system. Further advances in this work will also impact the practical science of hard magnets used in a variety of energy-related applications.

Reference: Er. Girt, Kannan M. Krishnan, G. Thomas, E. Girt and Z. Althunian, Jour. Mag. Mag. Mat., 231, 219 (2001).

Contact: Kannan M. Krishnan , Lawrence Berkeley National Laboratory
Phone: (510) 486-4614, Fax: (510) 486-5888, E-mail: Krishnan@lbl.gov

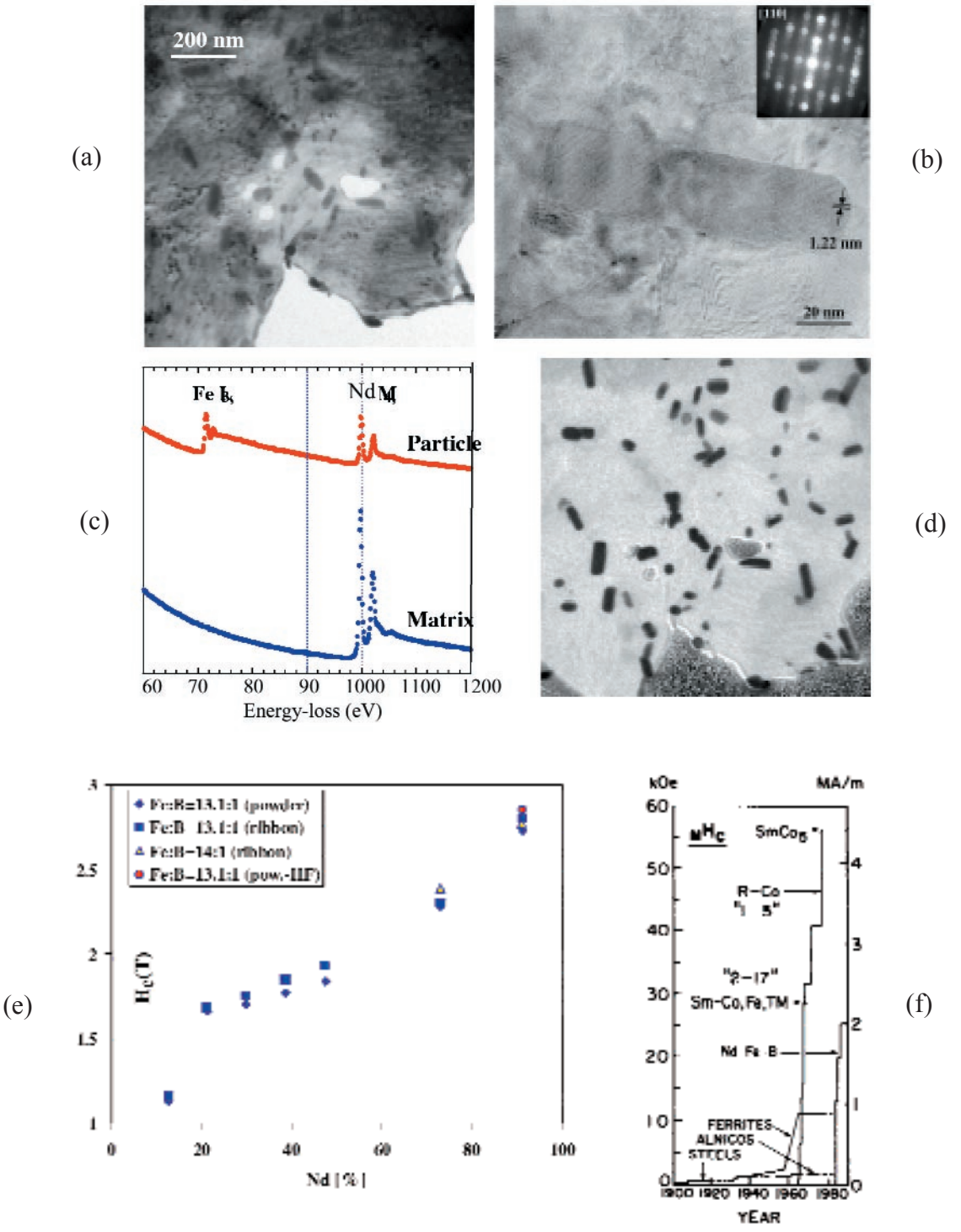

Figure. (a) Conventional electron micrograph of the Fe-Nd-B ribbon; (b) High resolution electron micrograph; (c) energy-loss spectrum ; (d) energy-filtered image using the Fe edge (notice better resolution of all particles); (e) increase in coercivity with Nd content; (f) historical comparison showing our results approaching ~83% of theoretical maximum.

Strong Collective Magnetism in Dipolar Nanocomposites

J. E. Martin *and* ***E. Venturini***
Sandia National Laboratories

Motivation—Improved high susceptibility and low conductivity magnetic materials are needed for high frequency transformers. Superparamagnetic nanoparticle materials are one possibility, but often have a rather low susceptibility. Our goal in this coordinated Center project is to use fields to manipulate the structure of nanoparticle composites to maximize the composite susceptibility, and to understand quantitatively the magnetism that results from dipolar interactions.

Accomplishment—We have demonstrated collective magnetism from dipolar interactions in dipolar nanocomposites consisting of superparamagnetic particles in a frozen matrix. These particles have a surface ligand that eliminates exchange coupling between spins on vicinal clusters. To demonstrate the effect of dipolar interactions on the magnetism of these materials, we have made composites wherein dipolar fields are maximized by assembly in a magnetic field, which causes particle chain formation while the matrix solidifies. Measurements on the solid sample show that the susceptibility along the chain direction is 4 times that normal to the chains, Fig. 1. The blocking temperature, which marks the onset of superparamagnetism, is also anisotropic, being larger in the chain direction, Fig. 2.

A Brownian dipole dynamics (BDD) code, written to gain insight into the magnetism of these composites, predicts susceptibility and blocking temperature anisotropies close to the measured values, though the susceptibility anisotropy is found to have a complex temperature dependence. Due to dipolar interactions, the magnetism of dipolar nanocomposites differs significantly from the Langevin theory (LT). The BDD code shows that at higher temperatures the susceptibility along the chains is enhanced relative to the LT, but as T approaches zero, the LT predicts a susceptibility divergence, whereas dipolar interactions suppress this, due to the existence of a negative magnetic ground state energy. Spin blocking might make the low-T susceptibility suppression kinetically inaccessible, but we have observed the enhancement regime parallel to the chains. Normal to the chains the BDD code shows a susceptibility suppression at all T, and we have observed this above the blocking transition. The shifts in the blocking temperature are reasonable in light of the computed magnetic ground state, which consists of antiparallel dipole chains. The increase in the blocking temperature parallel to the chains is thus due to the relatively high energy barrier for magnetization reversal in dipole chains.

Significance—These observations and computations constitute an important advance in understanding collective effects in dipolar nanocomposites. The observed susceptibility enhancements and low electrical conductivity could make these materials useful as high frequency transformers, and other applications are possible, including sensors and memory storage based on susceptibility alone.

Contact: J. Martin, Sandia National Laboratories/NM
Phone: (505) 844-9125, Fax: (505) 844-4045, E-mail: jmartin@sandia.gov

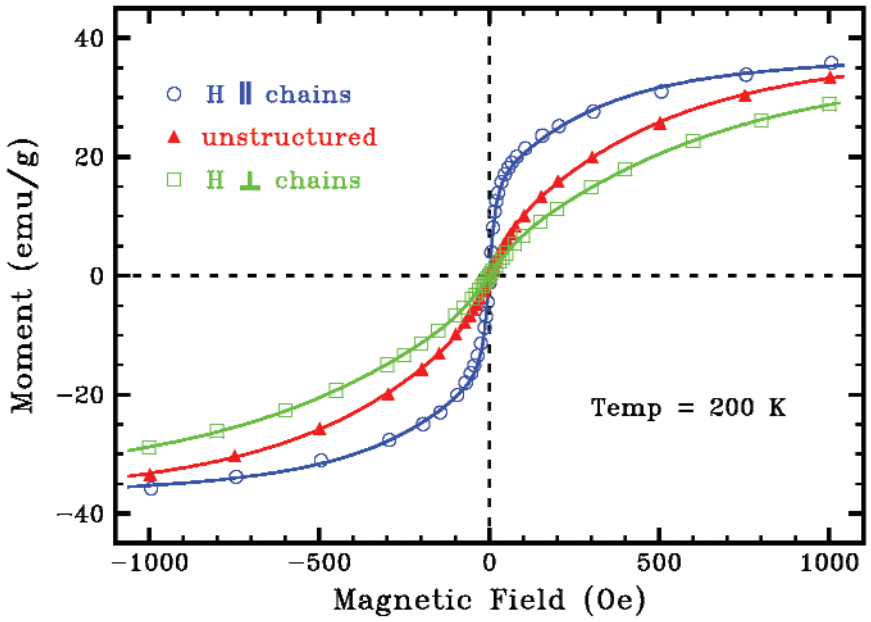

Figure 1. Magnetization curves showing strong anisotropy in a superparamagnetic nanoparticle composite structured by a magnetic field. The low-field response (susceptibility) is greatly enhanced in a field parallel to the chains compared to a perpendicular orientation or an unstructured composite.

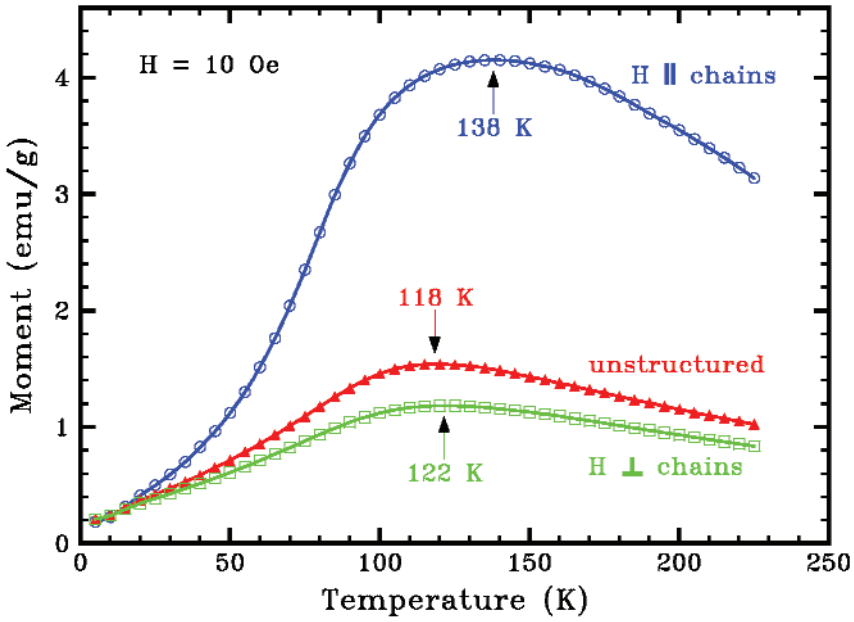

Figure 2. When a dipolar nanocomposite is warmed in a small magnetic field, it magnetizes via thermally-induced dipole hopping over magnetocrystalline energy barriers. The maximum moment occurs at the "blocking" temperature where the hopping time equals the experimental time of a few minutes. The hopping rate is significantly reduced by dipolar coupling in a structured nanocomposite.

Induced Molecular Ordering in Conducting Polymers

E.S. Peterson, *Idaho National Engineering and Environmental Laboratory*
G.J. Exarhos *and* ***J. Liu,*** *Pacific Northwest National Laboratory*
P. Braun*, University of Illinois*

Motivation—Structural organization in polymer films will lead to anisotropic physical properties that render such materials useful for microsensor applications, energy storage devices, and innovative semiconducting or optical emission devices. Achieving structural ordering over distances from nanometers to millimeters is quite difficult using conventional approaches. Innovative processing methods have recently been developed which drive formation of conducting polymer wires and slabs that exhibit a high degree of structural ordering in one dimension and over large distances. These methods rely on the electric field distribution in an electrochemical cell coupled with the solution templating chemistry (Fig. 1) that has been developed previously in this project to impart ordered porosity into a ceramic membrane material.

Accomplishment—For the first time, oriented and conducting polymer nanofibers, nanowires, and films with ordered nanoporosity over micrometer and larger length scales have been prepared electrochemically in three different systems. In one case a surfactant is added to the electrochemical bath that also contains a polymer precursor. The surfactant binds to the electrode surface and forms an ordered array that provides nucleation sites for the polymer phase which grows during electrolysis of the solution (Fig. 2). In the second case, an electrode surface is modified by depositing a colloidal crystal template or lyotropic liquid crystalline phase (Fig. 3). During current flow in the cell, the growing polymer phase fills up the interstices of the electrode template forming a polymer phase with ordered porosity when the template is removed. A third case demonstrates linear growth of a conducting inorganic polymer phase comprised of two distinct and serially grown polymer blocks (Fig. 4). This is done by first adding, then depleting one polymer precursor from the electrolysis solution, and then repeating the deposition upon addition of a second polymer precursor phase to the solution. The resulting conducting polymer wire shows rectifying properties analogous to that of a diode.

Significance—Research activities summarized here focus on understanding the mechanism that drives electrochemical polymerization of conducting polymers with oriented architectures. The mechanism is based upon the structure-directing properties of bound templating phases to an electrode surface where the polymerization reaction occurs. Processing methods developed here are used to grow ordered nanowires for potential application to energy transport, storage, and conversion technologies, sensor development, and as interconnects in microelectronic/microphotonic devices.

Contact: Greg Exarhos, Pacific Northwest National Laboratory
Phone: (509) 375-2440, Fax: (509) 375-2186, E-mail: greg.exarhos@pnl.gov

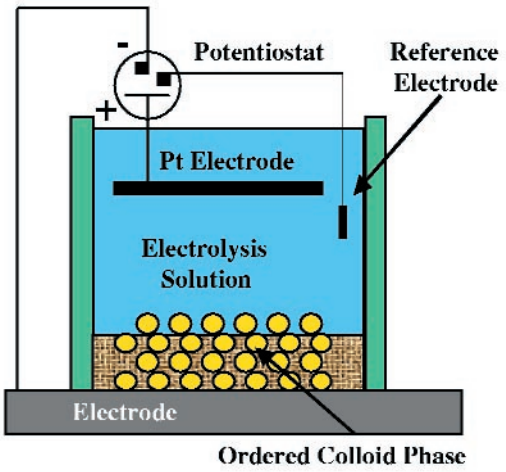

Figure 1. Electrochemical cell for growing ordered conducting polymer films.

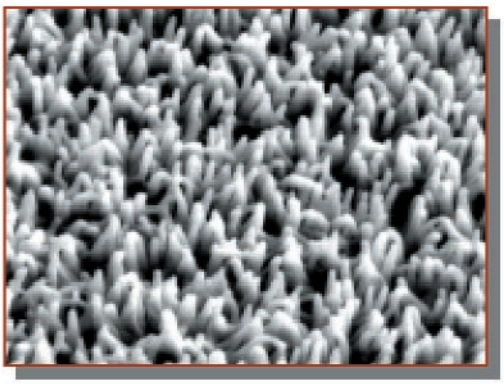

Figure 2. Surfactant-mediated growth of a conducting polymer film showing chain growth normal to the electrode surface.

1 μm

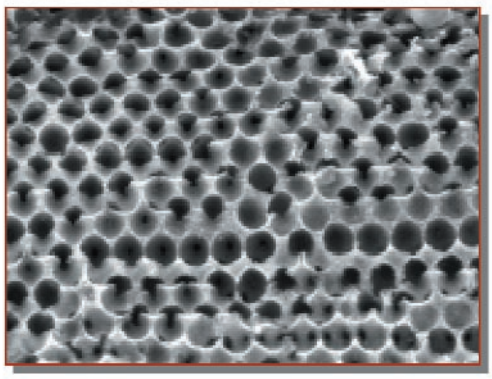

2μm

Figure 3. Electropolymerized polypyrrole around a colloidal crystal template followed by removal of the template, yielding a three-dimensionally periodic microporous structure.

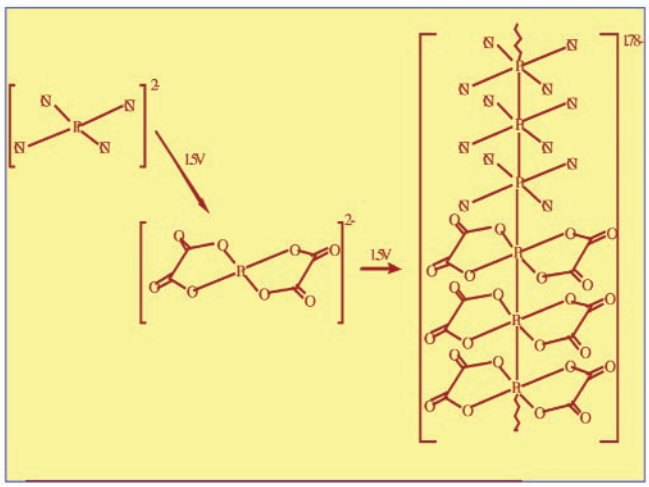

Figure 4. After complete polymerization of a solution containing the inorganic polymer precursor tetracyanoplatinate (II), a second precursor polymer, bisoxalatoplatinate(II) is added to the solution and electrolyzed leading to formation of a molecular wire with a rectifying junction (molecular diode).

Altered Phase Stability in Structured Block Copolymers

A. Habenschuss, M.-H. Kim and *G.D. Wignall,* Oak Ridge National Laboratory
F.S. Bates, C. Hardy and *T. Shefelbine,* University of Minnesota
JH Chang and *G.J. Exarhos,* Pacific Northwest National Laboratory

Motivation—Block copolymers can be made to spontaneously separate into distinct nanostructured domains. The phase-separated material can be used for semi-permeable membranes that require specific channel dimensions for transport of targeted molecules or in membranes that require both ionic and electronic conductivity. Molecular parameters that influence the attendant morphology include the polymer molecular weight, the relative block lengths, and the pairwise block-block interaction energies. With these parameters fixed, the resulting structure can only be altered with external variables such as temperature, electric field, or applied stress. However, addition of a homogeneous second phase can perturb the phase equilibrium resulting in a new morphology not accessible by that composition in the absence of the added phase. The goal of this project is to develop new methods for modifying phase stability regions in block polymer systems and to form hybrid materials that replicate the resident morphology of the phase-separated polymer.

Accomplishment—Addition of controlled amounts of polystyrene to a triblock copolymer, poly(isoprene-b-styrene-b-dimethylsiloxane), can vary the morphology from lamellar in the neat form to a variety of different structures. Phase morphologies determined by SAXS/SANS, TEM (Figure 1), and AFM have confirmed the predicted changes in the phase stability diagram.

A new process for preparing self-assembled ordered nanoporous materials is based upon the use of the copolymer as an organic templating phase. In this method, a ceramic precursor, tetraorthosilicate, is added to an acidified solution of the diblock copolymer, methoxy-polyethylene glycol-b-polyD, L-lactide, which has self-ordered into a packed micelluar phase where the micelle wall thickness is determined by the relative block lengths of the copolymer. The ceramic material then nucleates onto the ordered organic template and forms a replica following burnout of the organic template.

Significance—For the first time, a triblock copolymer that self-assembles into a lamellar phase has been driven to a number of other stable morphologies. The resulting structure of the polymer-copolymer hybrid is stabilized by the resident polymer chemistry and the amount of polymer phase present. The morphology of a self-assembled copolymer phase also can be replicated in a ceramic material by using the copolymer as a template. Both methods invoke localized molecular interactions between hydrophyllic and hydrophobic groups in the copolymer and between the copolymer and secondary phases to stabilize a new morphology.

Contact: A. Habenschuss, Oak Ridge National Laboratory
Phone: (423) 574-6018, Fax: (423) 576-5235, E-mail: habenschussa@ornl.gov

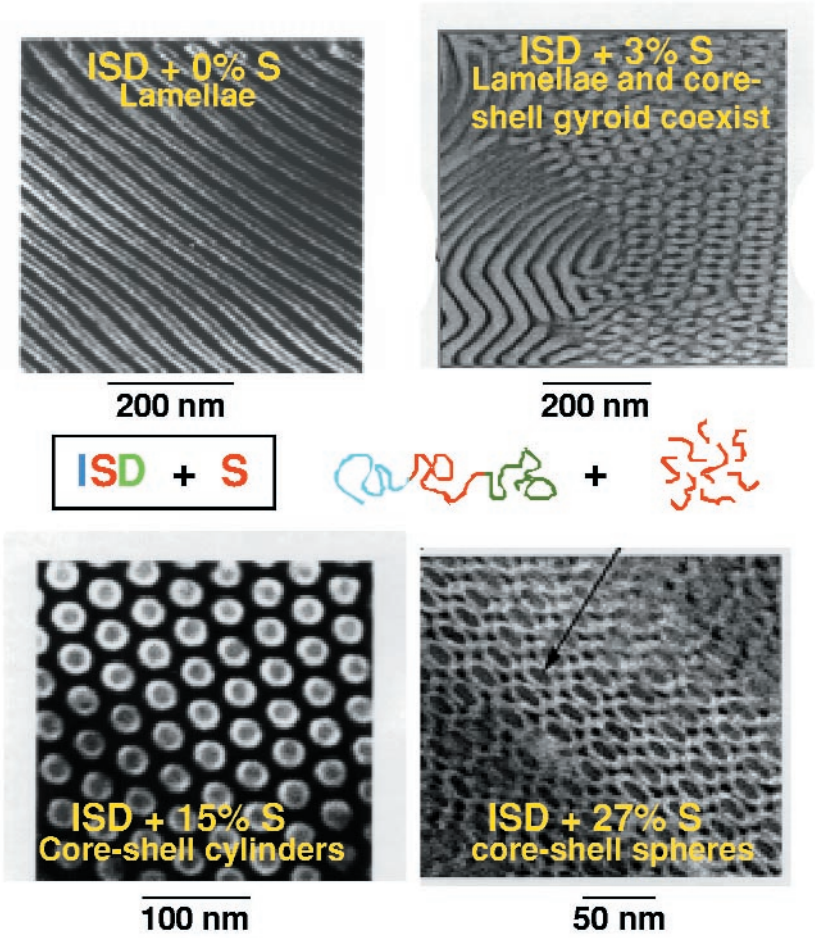

Figure 1. Resulting polymer hybrid morphologies upon addition as a function of polystyrene (S) additions to the triblock copolymer, poly(isoprene-b-styrene-b-dimethylsiloxane).

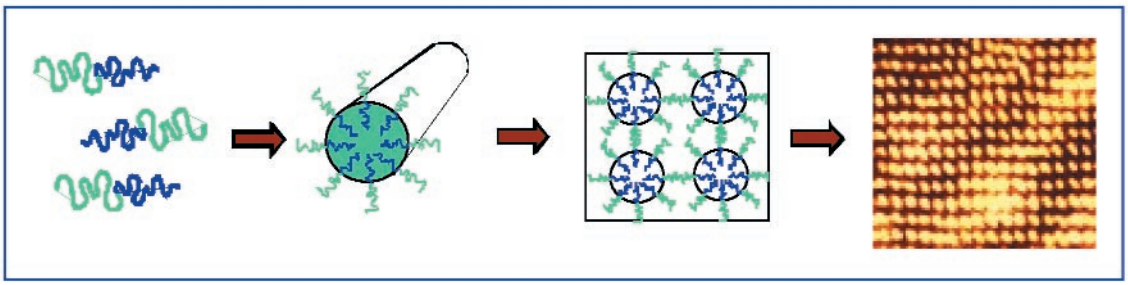

Figure 2. Self-assembled copolymer phase replicated in a ceramic. Block copolymers are designed and synthesized and allowed to self-assemble in solution. An added ceramic precursor phase nucleates and covers all surfaces in contact with the solution. The organic phase is extracted from the hybrid material.

Hybrid Ceramic Nanogel Composites for Controlled Release

B.C. Bunker, *Sandia National Laboratories*
J.H. Chang, G.J. Exarhos *and* ***J. Liu,*** *Pacific Northwest National Laboratory*
S. Malapragada, *Ames Laboratory*

Motivation—Intelligent protein delivery systems are required for applications ranging from controlled release of life-saving drugs to sequencing and separation operations. Development of smart composite release materials would have an immediate impact in these areas. A new generation of these hybrid systems is based on the incorporation of a temperature-responsive gel into an interconnected nanoporous matrix. A multifunctional gel would be designed to have a negative thermal expansion coefficient and exhibit a surface chemistry that changes reversibly from hydrophyllic to hydrophobic with temperature. Thus, proteins could be released from the gel as it is warmed either by a squeezing mechanism or by a surface debonding mechanism. Work in this Center project is focused on design and synthesis of such hybrid materials and their behavior as a function of heating.

Accomplishment—Hybrid composite materials were developed based upon the incorporation of poly(N-isopropyl acrylamide), PNIPAM, into a nanoporous silica phase. This was accomplished using two different methods. In one approach, a surfactant, polymer, and silica precursor were combined in solution to form a self-assembled bicontinuous phase. UV irradiation induced polymerization. Subsequent mild heating formed the hard silica phase containing the polymer. A second new "chain transfer" polymer synthesis method was developed and is based upon surface-initiated free radical polymerization of PNIPAM films which are bound to the pore surfaces by means of a silane coupling agent that acts as a tether. Both hybrid materials exhibit controlled and reversible release of proteins stimulated by change in the ambient temperature.

Significance—The "chain transfer" polymerization route has been used to form poly n-isopropyl acrylamide films on oxide membranes used for the reversible adsorption and release of proteins. Proteins stick to the PNIPAM when it is heated above its transition temperature of 35°C. When heater lines below the membrane are turned off, the proteins are rapidly released. The lower part of Fig. 1 is an image obtained in a fluorescence microscope of fluoroscene-tagged myoglobin being released from a single line less than one second after the heater is turned off. The use of temperature programming to switch protein adsorption on and off is being investigated for applications such as "on-chip" protein separations. A second example involving thermally induced release of antibiotic agents also has been demonstrated for the bicontinuous polymer silica network upon raising the temperature above a critical threshold (Fig. 2). Drug delivery ceases when the ambient temperature falls below the threshold. By designing the threshold to be slightly above body temperature, drug release can be turned on in response to fever.

Contact: Bruce Bunker, Sandia National Laboratories
Phone: (505) 284-244-6892, Fax: (505) 894-5470, E-mail: bcbunke@sandia.gov

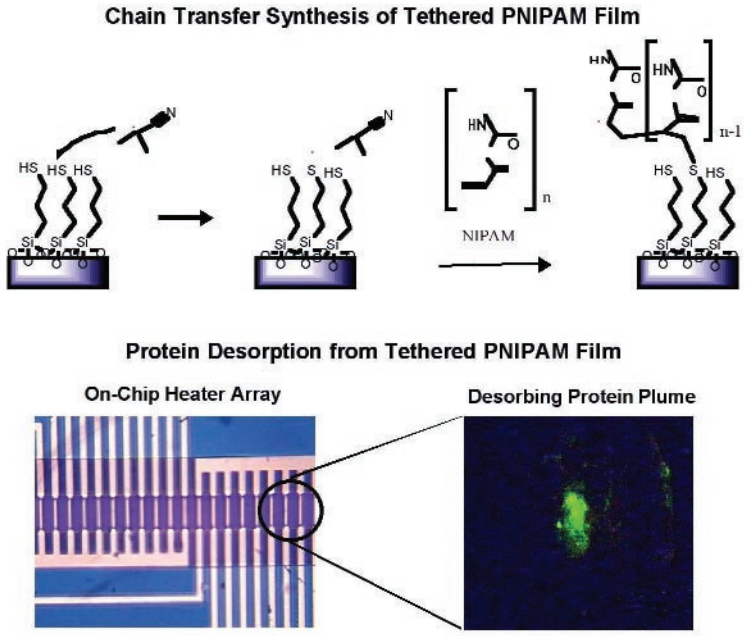

Figure 1. Synthesis and applications of tethered PNIPAM films. Top - Free radicals transferred to tethered thiol promote surface polymerization. Bottom - PNIPAM films polymerized on heater membrane at left (Au heater line width = 50 μm). Green in right image is fluorescent myoglobin being released from central heater line 0.5 seconds after the heat was turned off.

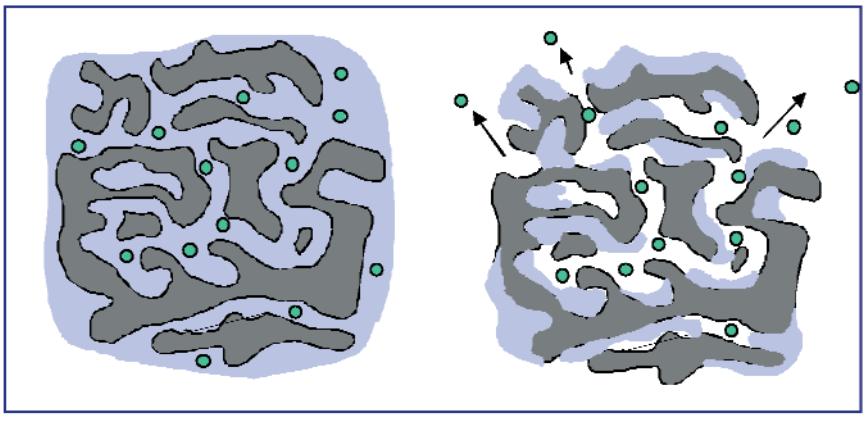

Figure 2. Antibiotic binding to a nanogel hybrid below the critical temperature (left); release of the antibiotic from the nanogel hybrid above the critical temperature (right).

Reducing the Thermal Expansion Anisotropy of Mo_5Si_3-based Molybdenum Silicides

J. H. Schneibel, C. L. Fu, C. J. Rawn *and* ***T. R. Watkins***
Oak Ridge National Laboratory

Motivation—The intermetallic Mo_5Si_3 has potential as an ultra-high temperature, oxidation resistant structural material. Previous experiments by Chu et al. and *ab initio* calculations by Fu et al. indicated a high anisotropy in the coefficients of thermal expansion (CTE) along the crystallographic *a* and *c* directions. The high thermal expansion along the *c*-axis was attributed to chains of closely spaced Mo atoms which contribute to high anharmonicity. Very importantly, our understanding of the physical mechanisms for the high CTE anisotropy leads to strategies for reducing the anisotropy. We can either stretch the Mo chains by inserting large atoms on sites other than the chain sites or replace Mo atoms in the chains with smaller atoms. The motivation for the experimental research presented here is to (a) verify the validity of the theoretical ideas and (b) minimize micro-cracking in Mo_5Si_3-base polycrystals by reducing the CTE anisotropy.

Accomplishment—Figure 1 shows a (100) plane of Mo_5Si_3 illustrating the chains of closely spaced Mo atoms. Because of its large size Nb is not expected to substitute for Mo atoms in the chains, but rather on other Mo sites thereby stretching the Mo chains. This site preference has been confirmed by model calculations. Consequently, as Nb is added to Mo_5Si_3 the coefficient of thermal expansion in the *c*-direction, CTE(*c*), decreases. The ratio of the CTEs in the *c* and *a* directions decreases dramatically as Nb is added (Fig. 2). The measured results are consistent with the *ab initio* calculations that show that the CTE ratio is reduced from 2 for Mo_5Si_3 to 1.5 for Mo_4NbSi_3. Consistent with the reduction in the CTE anisotropy, optical micrographs of polished sections (Fig. 3) show much less micro-cracking in a Nb-containing alloy as compared to binary Mo_5Si_3. Figure 2 also shows a datum point for a V-containing alloy, $(Mo_{0.8}V_{0.2})_5Si_3$. Vanadium is smaller than Mo. By substituting for the Mo atoms in the chains, V reduces the CTE in the *c*-direction, and the CTE ratio from a value of 2 to a value of 1.5. Our results show clearly that the interaction between *ab initio* modeling and experiment has advanced our understanding of the changes in the CTEs of 5-3 based molybdenum silicides.

Significance—This work has developed a scientific basis for reducing the CTE anisotropy of Mo_5Si_3. It is likely that alloying elements other than Nb or V can be used to reduce the CTE anisotropy of Mo_5Si_3. Quaternary alloys can also be considered. This opens up the possibility of reducing the CTE ratio to the preferred value of 1 and producing micro-crack free alloys based on Mo_5Si_3. Our versatile model can also be applied to numerous other compounds with anisotropic structures.

Contact: J. H. Schneibel, Oak Ridge National Laboratory
Phone: (865) 576-4644, Fax: (865) 574-7659, E-mail: schneibeljh@ornl.gov

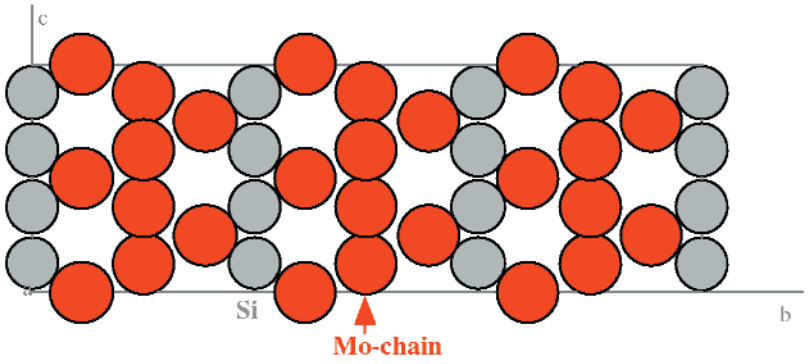

Figure 1. (100) plane of Mo_5Si_3 illustrating chains of closely spaced Mo atoms in the *c*-direction.

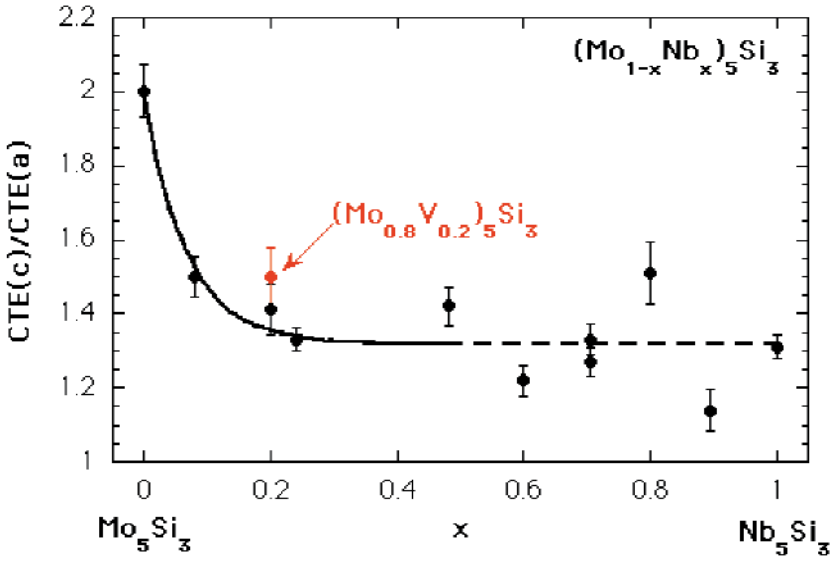

Figure 2. Additions of Nb or V to Mo_5Si_3 reduce the ratio of the thermal expansion coefficients, CTE(*c*)/CTE(*a*).

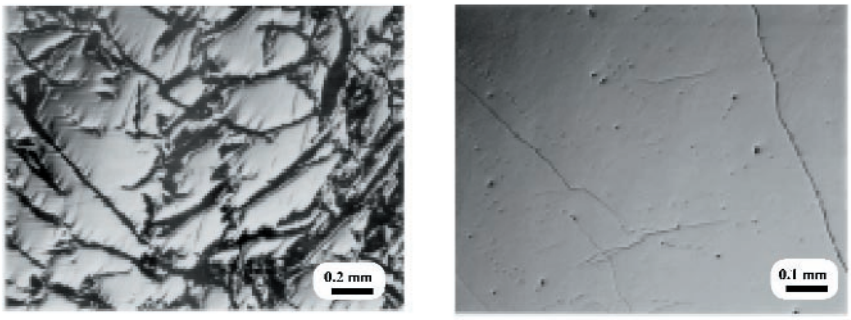

Figure 3. Additions of Nb reduce the serious micro-cracking of Mo_5Si_3 by reducing the CTE anisotropy.

Development of High-Toughness Mo-12Si-8.5B (at.%) Intermetallic Alloys for Elevated-Temperature Applications

H. Choe *and* ***R. O. Ritchie,*** *Lawrence Berkeley National Laboratory*
J. H. Schneibel, *Oak Ridge National Laboratory*

Motivation—The quest for structural materials that can operate at higher and higher temperatures remain a persistent challenge in materials science. One candidate system is $MoSi_2$-based silicides, which have good oxidation resistance up to 1700°C and relatively easy processibility; however, like many ordered intermetallics, they are plagued by poor ductility and very low fracture toughness. Boron-containing molybdenum silicides have been the focus of significant research of late due to their potentially superior low-temperature "pest" resistance and high-temperature oxidation resistance due to the formation of borosilicate glass. Of the various multiphase Mo-Si-B intermetallic systems available, alloys with compositions of Mo-12Si-8.5B (at.%), which contain Mo, Mo_3Si, and Mo_5SiB_2 (T2) phases (Figure 1), are anticipated to have higher toughnesses because of the presence of the relatively ductile α-Mo phase. In this study, we examine the ambient to high (1300°C) temperature fracture toughness (R-curve) and fatigue-crack growth characteristics of Mo-12Si-8.5B, with the objective of discerning the salient mechanisms governing crack growth.

Accomplishment—The fracture toughness (Figure 2) and fatigue-crack growth resistance (Figure 3) of the Mo-12Si-8.5B alloy are substantially higher than monolithic $MoSi_2$ and $MoSi_2$ reinforced with Nb spheres both at ambient and elevated temperatures. This alloy displays a relatively high *intrinsic* (crack-initiation) toughness at 800 up to 1200°C (~10 MPa√m) due to *crack trapping* toughening mechanism by α-Mo phase, but only limited *extrinsic* R-curve (crack-growth) toughness. Although the lack of extrinsic toughening mechanisms is not necessarily beneficial to quasi-static properties, it does imply in a brittle material that it should show only minimal susceptibility to premature failure by fatigue, as is indeed observed at temperatures from ambient to 1300°C. Of particular significance is that both the fracture toughness and the threshold stress intensity for fatigue are increased with increasing temperature over this range. This remarkable property is associated with the onset of additional toughening mechanisms that become active at elevated temperatures, specifically involving *crack bridging* by the α-Mo phase and extensive *microcracking* primarily in the Mo_5SiB_2 phase as shown in Figure 2.

Significance—The boron-modified molybdenum silicide alloy, Mo-12Si-8.5B, can be processed to be considerably tougher (>10 MPa√m) and more fatigue resistant (fatigue threshold ~7 MPa√m) than monolithic $MoSi_2$ and Nb-spheres reinforced $MoSi_2$. Moreover, its crack-growth resistance, in both fracture and fatigue, progressively increases with increase in temperature up to 1300°C. Current studies are focusing on several new microstructures designed to create an optimal balance of high-temperature oxidation and mechanical properties.

Contact: R. O. Ritchie, Lawrence Berkeley National Laboratory
Phone: (510) 486-5798, Fax: (510) 486-4881, E-mail: roritchie@lbl.gov

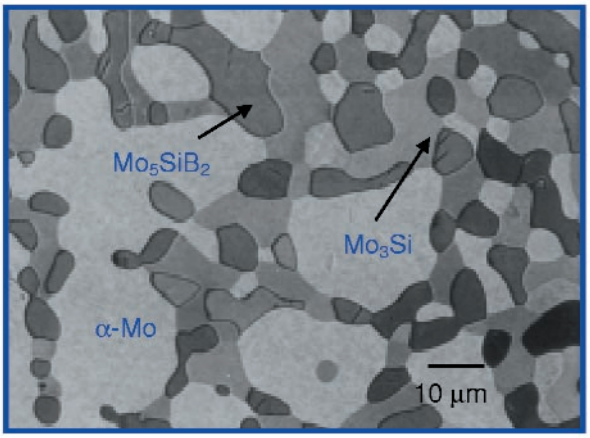

Figure 1. Scanning electron micrograph of the Mo-12Si-8.5B (at.%) alloy, showing α-Mo particles in the Mo_3Si/Mo_5SiB_2 matrix.

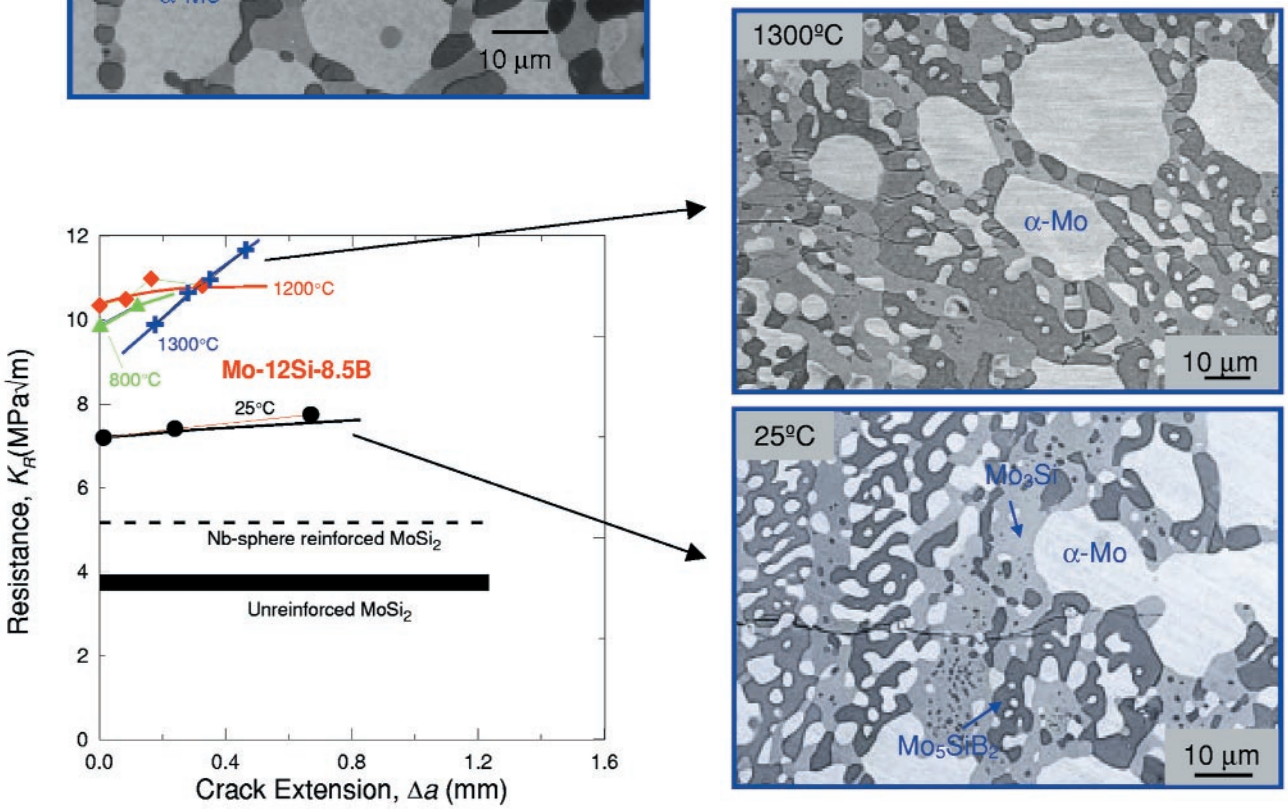

Figure 2. Fracture toughness behavior, in the form of K_R (Δa) crack-growth resistance curves, for Mo-12Si-8.5B alloy both at ambient and elevated temperatures, as compared to monolithic $MoSi_2$ and $MoSi_2$ reinforced with Nb spheres.

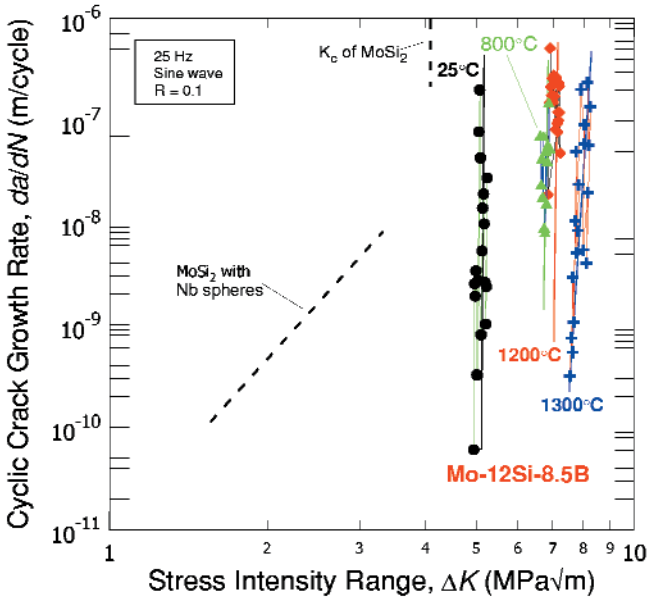

Figure 3. Cyclic fatigue-crack propagation data of Mo-12Si-8.5B alloy as a function of applied ΔK at 25°C, 800°C, 1200°C, and 1300°C, compared to monolithic $MoSi_2$ and $MoSi_2$ reinforced with Nb spheres.

Molybdenum-Silicon-Boron Intermetallics with a Continuous Molybdenum Matrix

J. H. Schneibel, *Oak Ridge National Laboratory*
M. J. Kramer, *Ames Laboratory Hughes*

Motivation—The fracture toughness of ultrahigh temperature alloys consisting of the phases α-Mo, Mo_3Si (A15 phase) and Mo_5SiB_2 (T2 phase) is determined not only by the volume fraction, but also by the spatial distribution of the α-Mo phase. A continuous α-Mo matrix resulting in a microstructure similar to that of cobalt-bonded tungsten carbide is particularly desirable. Consolidating coarse Mo_3Si and Mo_5SiB_2 particles with fine Mo powder was found to be only partially successful for creating a continuous Mo matrix. Forming a thin Mo-coating on the surfaces of Mo-Si-B powder particles prior to consolidation is expected to lead to the desired microstructure.

Accomplishment—A Mo-20Si-10B (at. %) alloy consisting of the phases Mo_3Si and Mo_5SiB_2 was annealed at 1600°C in vacuum at a pressure of 10^{-3}Pa. X-ray diffraction and electron probe analysis confirmed that the surface was enriched in Mo. Based on well-known thermodynamic data this effect is explained as follows: in a low oxygen partial pressure environment the decomposition products of silicon bearing alloys contain SiO rather than SiO_2. Since SiO is volatile at 1600°C it sublimes continuously during the annealing process. As a result, the surface loses silicon and becomes enriched in α-Mo which is stable under these conditions. Since the Si must diffuse through an ever thickening Mo layer parabolic rate kinetics are expected. Figure 1 shows quantitative x-ray diffraction data for the volume fraction of α-Mo formed on the surface of coarse Mo-20Si-10B powder. As expected the increase in the volume (or thickness) of the Mo-enriched layer is proportional to the square root of the time supporting the hypothesis that silicon diffusion is the rate limiting process. Figure 2 confirms that a fully dense specimen with a continuous metal matrix can be fabricated by hot isostatic pressing of vacuum-annealed powders. This process is easily controlled by varying the size of the powder particles and the time of anneal, thus providing different α-Mo volume fractions and α-Mo ligament widths. In this way the fracture toughness can be controlled within a wide range.

Significance—The processing technique established in this research enables us to produce microstructures that can be obtained neither by melting and casting nor by conventional powder processing. By varying the volume fraction and the ligament size of the α-Mo matrix in the consolidated material a wide range of mechanical properties can be obtained. This high degree of microstructural control also enables us to control the type of toughening mechanism. The microstructural control has thus direct consequences for the work by Ritchie and collaborators on static and fatigue crack propagation in Mo-Si-B alloys carried out under the auspices of this program.

Contact: J. H. Schneibel, Oak Ridge National Laboratory
Phone: (865) 576-4644, Fax: (865) 574-7659, E-mail: schneibeljh@ornl.gov

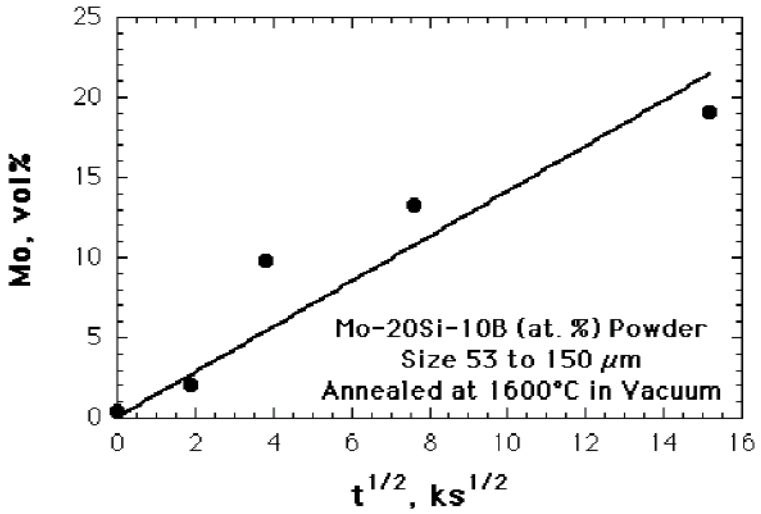

Figure 1. The surface of molybdenum silicide powder becomes Mo-enriched during annealing in vacuum. The α-Mo volume fraction follows a parabolic rate law.

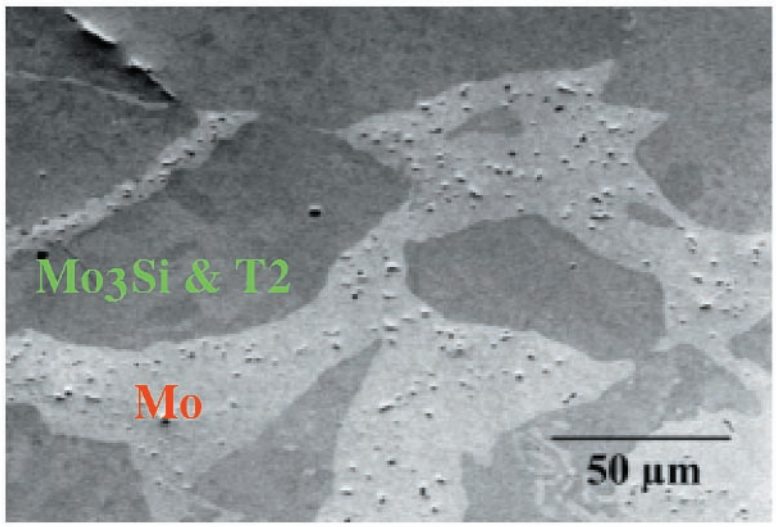

Figure 2. Mo-20Si-10B powder with Mo-enriched surfaces was consolidated by hot isostatic pressing. The light regions in the polished section shown indicate a continuous α-Mo matrix. This microstructure is desirable because it enhances the fracture toughness.

Ferroelectric Properties of $KTaO_3/KNbO_3$ Superlattices by Atomistic Simulation

M. Sepliarsky, S. R. Phillpot *and* ***D. Wolf,*** *Argonne National Laboratory*
M. G. Stachiotti *and* ***R. L. Migoni,*** *Univ. of Rosario, Argentina*

Motivation—Semiconductor and magnetic superlattices have long been exploited for their novel properties. Driven by the vision of creating artificial structures with ferroelectric and piezoelectric properties unobtainable in either single-component materials or in solid solutions, attention is now also focussing on superlattices involving ferroelectric perovskites. One type of superlattice receiving particular attention consists of alternating layers of a perovskite ferroelectric and a perovskite paraelectric. Particularly well-characterized (by members of this CSP Center project) are $KTaO_3/KNbO_3$ superlattices. Atomic-level simulation should be able to provide important insights into the properties of these multilayer systems.

Accomplishment—We have developed and validated an atomic-level approach to the simulation of the phase behavior of perovskite materials. We chose $KTa_xNb_{1-x}O_3$ (KTN) as a model system, with x=0 corresponding to $KNbO_3$, which exhibits four solids phases (rhombohedral, orthorhombic, tetragonal and cubic, the first three being ferroelectric) and x=1 corresponding to $KTaO_3$, which remains cubic at all temperatures. We have used atomic-level simulation methods to determine the zero-temperature structure and properties of coherent $KNbO_3/KTaO_3$ superlattices. We found that the in-plane behavior is essentially bulk-like with an abrupt jump in the polarization at the interfaces. By contrast, the polarization in the modulation direction is continuous through the interfaces with the interior of the $KTaO_3$ layers remaining polarized for modulation lengths of up to 160 unit cells. The zero-frequency dielectric constant in the modulation direction has a similar magnitude to that of $KNbO_3$. An investigation of the switching behavior showed that for modulation lengths greater than 24 unit cells, each $KNbO_3$ layer behaves essentially independently. For modulation lengths less than twelve unit cells, the $KNbO_3$ layers interact so strongly with each other that, the superlattice essentially behaves as a single artificial structure.

Significance—It has been demonstrated that atomic-level simulation is capable of investigating materials-science issues in ferroelectric perovskites at the atomic scale. The insights obtained in our studies are an essential first step towards a systematic understanding of the intrinsic properties of ferroelectric/paraelectric heterostructures.

Contact: Simon R. Phillpot, Argonne National Laboratory
Phone: (630) 252-5480, Fax: 252-4289, E-mail: phillpot@anl.gov

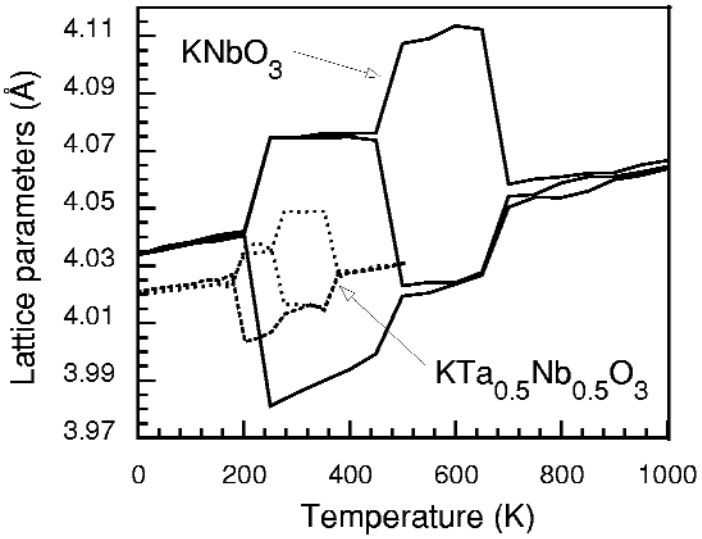

Figure 1. The phase diagrams of $KNbO_3$ (solid lines) and $KTa_{0.5}Nb_{0.5}O_3$ (dotted lines) determined from molecular-dynamics simulation are very similar to those determined experimentally.

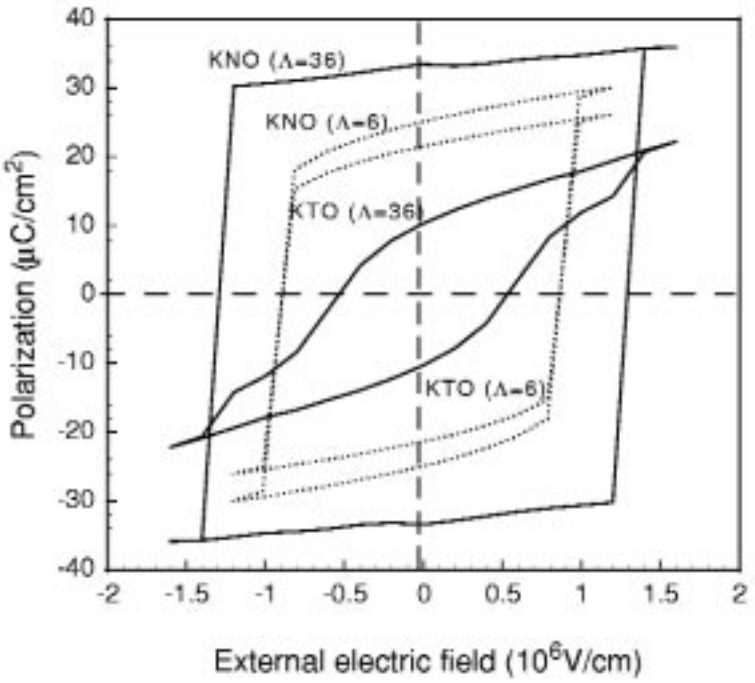

Figure 2. Calculated hysteresis loops for the $KNbO_3$ (KNO) and $KTaO_3$ (KTO) layers in KNO/KTO superlattices with Λ= 36 (solid lines) and the Λ=6 (dotted lines).

Synthesis and Characterization of Lanthanide Doped Lead Zirconate Titanate

T. J. Boyle, J. T. Dawley, B. A. Tuttle, P. G. Clem, M. A. Rodriguez,
T. Dunbar and W. F. Hammetter, *Sandia National Laboratories*
G. L. Brenneka, *Univ. of Missouri Rolla*

Motivation—Appropriate incorporation of aliovalent dopants into lead zirconate titanate (PZT) materials is used to optimize dielectric, electro-optic and piezoelectric properties. For PZT thin films, La doping has been shown to enhance fatigue resistance and to increase breakdown strength at high temperatures (125 °C). We have further investigated the effects of doping PZT using the lanthanide (Ln) cation series. The Ln series is ideal to develop a science- based understanding of the impact of dopant ionic size since the cation size systematically decreases from La^{+3} to Lu^{+3} by ~ 0.17 Å. For $BatiO_3$, which has a similar simple perovskite structure as PZT, larger ions were shown by EPR analyses to preferentially occupy the A-site of the perovskite lattice and act as donors. As ionic size decreased, the Ln dopants become amphoteric, exhibiting both A and B site occupation. With further reduction in ionic size, the lanthanide ions preferentially occupied B-sites and acceptor behavior was exhibited. A primary reason for investigating this under explored material system is the possibility of synthesizing PZT based films with superior polarization (P_r), dielectric constants (ε), fatigue, retention and breakdown performance.

Accomplishment—Due to the flexibility of Sandia's solution chemistry process, illustrated in Figure 1, we were able to synthesize PLnZT solutions over the entire lanthanide series. PZT films with the sixteen different lanthanide dopants were fabricated by standard spin-pyrolysis deposition methods. Each of the films deposited on Pt coated Si wafers was found to be single-phase perovskite by X-ray diffraction. EPR characterization of solution-derived, Gd-doped PZT gel particles indicated that these particles were on the boundary of donor - amphoteric behavior.

The fatigue performance for different dopants is shown in Figure 2. Films doped with amphoteric dopants (e.g., Dy) exhibited better fatigue performance than films with acceptor dopants (e.g., Lu). Donor doping reduces the number of oxygen vacancies in the PZT system, and thereby, reduces the number of electron trap sites that pin domain walls, which reduces the switchable polarization. The fatigue performance for the Dy-doped film is substantially better than for the similarly processed, industry standard La-doped films. The Dy-doped films have essentially no fatigue over a range of 10^{10} switching cycles. The reasons why some amphoteric dopants exhibit better fatigue behavior than donor dopants are under investigation.

Significance—Improved properties of the lanthanide doped PZT films will enable new piezoelectric and nonvolatile memory technologies. This study has led to a better materials understanding of the effects that dopants have on the atomic structure and the related macroscopic properties of PZT films.

Contact: Timothy J. Boyle, Sandia National Laboratories
Phone: (505) 272-7625, Fax: 505-272-7336, E-mail: tjboyle@sandia.gov

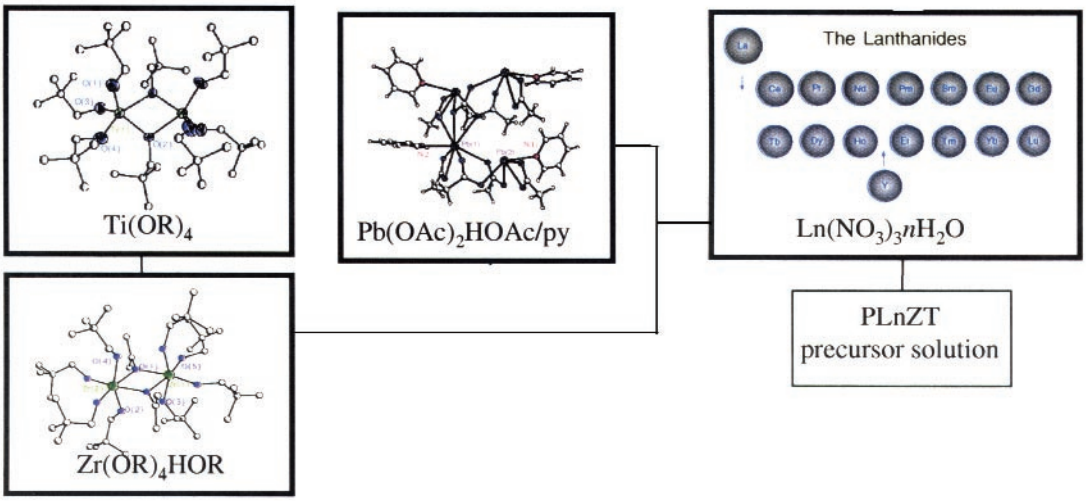

Figure 1. Schematic representation of precursor solution synthesis.

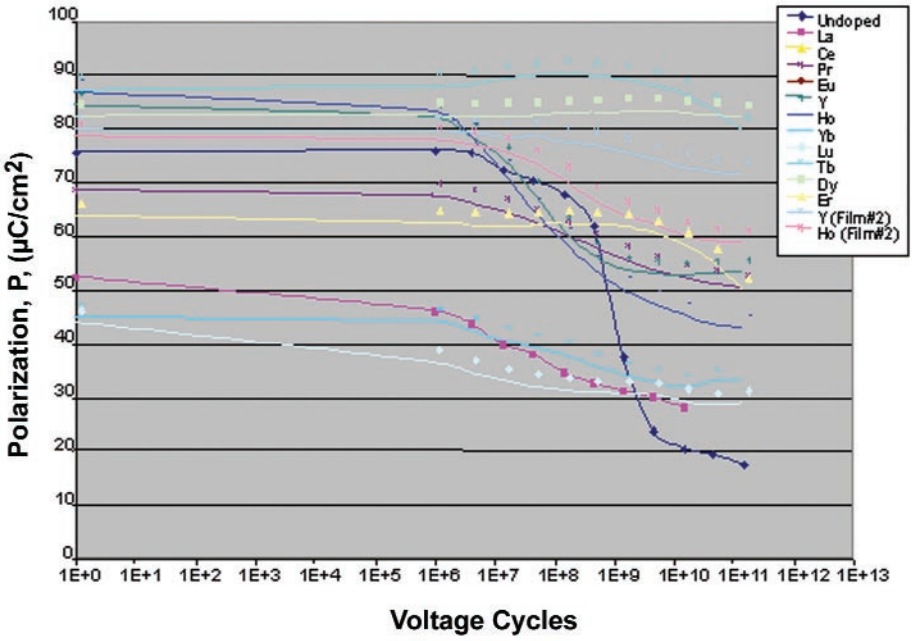

Figure 2. Polarization fatigue behavior of lanthanide doped PZT (PLnZT) films as a function of dopant.

Studies of Oxidation Processes in Conductive Ti-Al Diffusion Barrier Layers via In Situ Nanoascale Surface Sensitive Analytical Techniques

O. Auciello and A.M. Dhote, *Argonne National Laboratories*
R. Ramesh, *University of Maryland*

Motivation—Understanding growth and oxidation processes of conducting diffusion barrier layers represents both a scientific challenge and a technologically critical step in the integration of ferroelectric capacitors with complementary metal oxide semiconductor (CMOS) devices for the realization of high density non-volatile ferroelectric random access memories. To address the challenges, we have investigated a new Ti-Al layer as a thin film barrier with relatively low resistivity (~300 μΩ cm). This material can act as both a diffusion barrier and a bottom electrode, replacing conventional electrode-barrier structures such as Pt/TiN or Ir/TiN. The scientific challenge is to understand oxidation processes of Ti-Al layers at the atomic scale. We also demonstrated that a $La_{0.5}Sr_{0.5}CoO_9$ (LSCO)/ amorphous a-Ti-Al heterostructure exhibits desirable ohmic behavior, while an LSCO/ polycrystalline Ti-Al (c-Ti-Al) layer with a columnar microstructure is non-ohmic. However, our prior work did not provide information on the fundamental processes underlying the interaction of oxygen atmospheres with the Ti-Al layer.

Accomplishment—We have now obtained insights into the oxidation processes of Ti-Al layers using a unique integrated ion beam sputter-deposition (IBSD) / *in-situ* mass spectroscopy of recoil ions (MSRI) / X-ray photoelectron spectroscopy (XPS) system. MSRI provides atomic-scale information of species on the a-Ti-Al surface, via secondary ions ejected by impact of the probing ions, while XPS yields information on the chemical environment at the a-Ti-Al surface. Figure 1 shows the variation of MSRI signals for individual atomic species evolving from the a-Ti-Al surface and the Ti^+/Al^+ peak ratio as a function of oxidation temperature. Practically no variations in intensities of the Ti^+, Al^+, O^+ and Ti^+/Al^+ ratio signals occur up to 600°C. However, there are substantial increases of the MSRI Ti^+, and Ti^+/Al^+ ratio signals as the substrate temperature changes from 600°C to 700°C. The large increases in the Ti^+/Al^+ ratio and Ti^+ signals result from metallic Ti species segregated to the surface of the a-Ti-Al layer due to oxidation to TiO_2. The segregated Ti layer is only one to two monolayers thick as indicated by the sharp Ti peak. The increase in the secondary ion signal (e.g., Ti^+) upon oxidation is due to a lower rate of electron transfer from the oxidized surface to the departing ions. *In-situ* XPS analysis provided insights into the chemical attachment of oxygen to the individual atomic species. Fig. 2 shows XPS spectra of the a-Ti-Al surface around the Ti [$2p_{1/2}$, $2p_{3/2}$] and TiO_2 [$2p_{1/2}$, $2p_{3/2}$] peaks before (spectrum at 20°C) and after free surface oxidation [$P(O_2)= 5x10^{-4}$ Torr] at 400°, 500°, 600° and 700°C. The XPS peaks (Fig. 2a) correspond to metallic Ti for the surface of an a-Ti-Al layer exposed to 10^{-3} Torr of oxygen at 400-600°C. The peaks observed after increasing T from 600°C to 700°C are correlated with the presence of TiO_2 formation on the a-Ti-Al surface. In addition, the evolution of the XPS oxygen peak [Fig 2b] shows a one-to-one correlation with the evolution of the Ti and TiO_2 peaks in Fig. 2. Thus the data indicate that the a-Ti-Al layer is stable until 600°C in oxygen.

Significance—Barriers such as Ti-Al can enable the integration of ferroelectric capacitors with MOS devices for high density non-volatile ferroelectric random access memories.

Contact: Orlando Auciello, Argonne National Laboratory
Phone: (630) 252-1685; Fax: 630-252-4289; E-mail: auciello@anl.gov

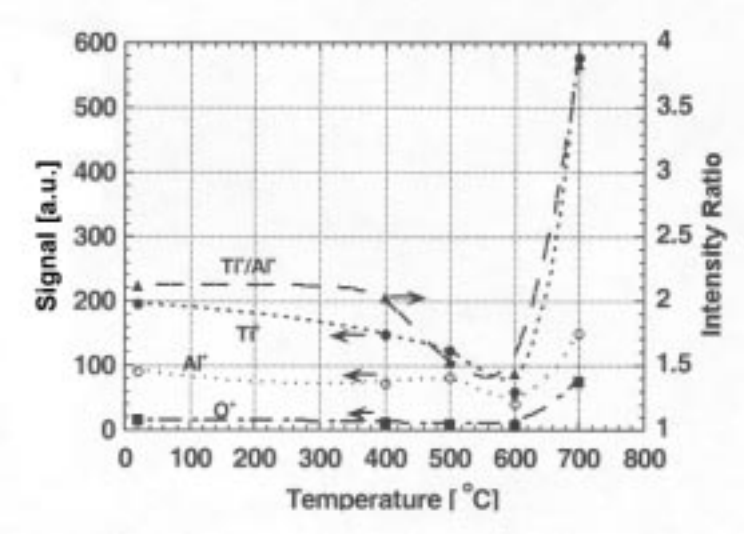

Figure 1. Variations of MSRI signals (counts) for different species as a function of oxidation temperature during exposure of an a-Ti-Al thin film on a p-Si surface to an oxygen atmosphere in the range 50 -700 °C. Also shown is the ratio of the Ti^+ to the Al^+ signal.

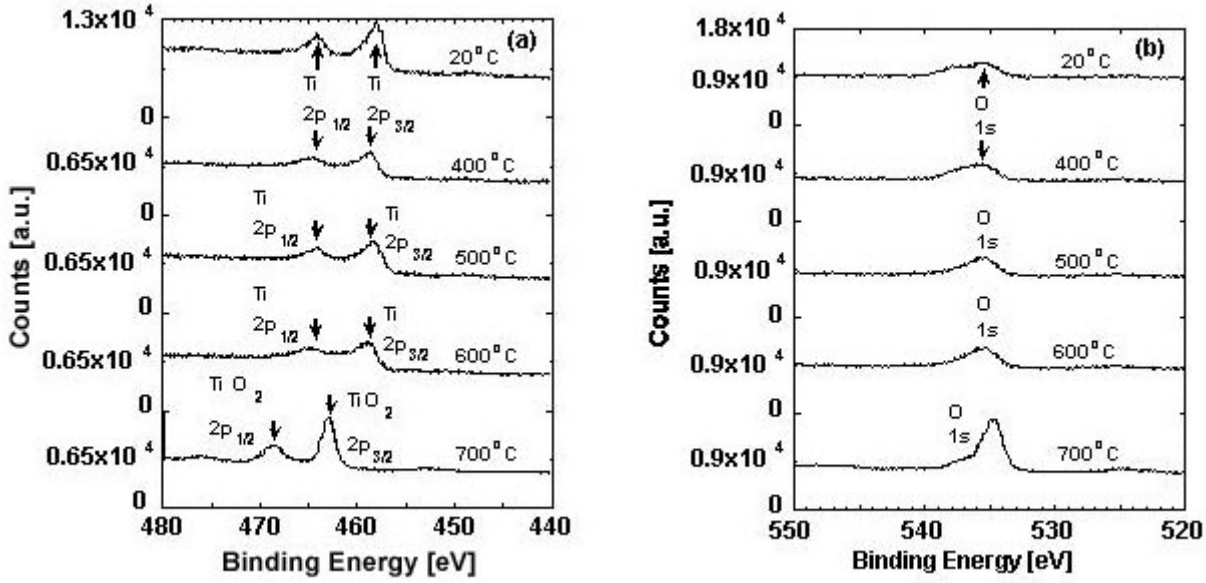

Figure 2. XPS spectra of a-Ti-Al surface around the metallic Ti [$2p_{1/2}$, $2p_{3/2}$] and TiO_2 [$2p_{1/2}$, $2p_{3/2}$] peaks (a); and the O[1s] peak (b) as a function of oxidation temperature for an a-Ti-Al barrier layer on p-Si.

Modeling the Dynamics of Site Interactions in the Localized Corrosion of Aluminum

R. G. Kelly, *University of Virginia*
H. Isaacs, *Brookhaven National Laboratory*

Motivation—Localized corrosion properties have been studied for a wide range of engineered alloys, including pitting corrosion in aluminum alloys. Pitting corrosion occurs at microscopic defects on the metal surface with the establishment of potential and chemical gradients in the solution surrounding the corrosion sites. Experimental measurements, like the optical images in Figure 1, show evidence of pit interactions that contribute to sustaining corrosion processes and leading eventually to material failure. Statistically based computation, like surface response methods, show promise at elucidating these inter-pit dynamics and providing a predictive framework for understanding corrosion behavior and alloy stability.

Accomplishment—Our approach is to use a two-dimensional, time transient mass transport model to examine the interaction between two activated pits in aluminum. The relative importance of various chemical and physical parameters are determined by parametric variation using a design of experiment format determined by surface response algorithms. This determination of parameter significance allows predictive models to be developed to explain how pits interact and whether corrosion is sustained.

Parameters used in our simulations include the individual pit corrosion rates, local pHs, the transition pHs (pit stability pH), and the pit separation distance. Pits were initiated by lowering the chosen active site pH below that of the transition pH. The initial pit was activated at the onset of the experiment, subsequently followed by the initiation of the second pit at a determined time. The time-rate of change in pH of the second pit after four minutes from its initiation determined the pit's stability. If the pH was decreasing, the second pit was undergoing stable corrosion, whereas if the pH was increasing, the second pit was determined to be unstable and would soon stop actively corroding. The image in Figure 2 shows the results of a simulation where favorable values of parameters produce a stable second pit.

Based on multiple simulations, a linear model was developed based on correlating the pit parameters with the formation of a stable second pit. It was found that the three most important factors were the assumed transition pH (range studied 2.5 to 4), the starting pH of the second pit (range studied 1 to 3), and the relative dissolution rate of pit 2. A model that included interaction terms as well as the initial pH of pit 1 leads to a linear model with ten terms and an R^2 value of 0.92 as shown in Figure 3. Of equal interest was the determination that neither the pit separation (range studied 0.4 to 1.2 cm) nor the time delay before the second pit is initiated (range studied 300-2100 sec) were predictive in the stability of the second pit under the conditions studied.

Significance—This greater importance of local pH, the transition pH and the initial dissolution rate indicates the long-range effects of the chemical interactions in pitting. By adding the electrochemical behavior of the pit and surrounding material, a complete model of the pit interactions will be achieved, allowing a more complete simulation of the experimental results. In addition, information not accessible experimentally (e.g., local chemistry) can be calculated.

Contact: Robert G. Kelly, University of Virginia
Phone: (804) 982-5783, Fax: (804) 982-5799, E-mail: rgkelly@virginia.edu

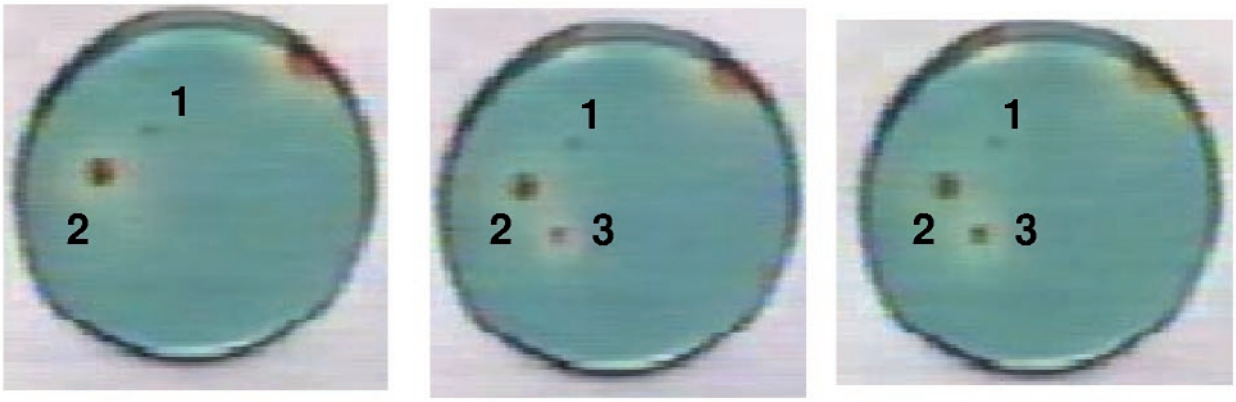

Figure 1. Time-dependent evolution of pits (8 min between frames) on an Al 1100 surface with a de-oxygenated Agar gel containing a pH indicating dye (red indicates a corroding pit) and 1 M NaCl. Pit 1 has grown and stopped, followed by pit 2, which continues to grow as pit 3 initiates and grows.

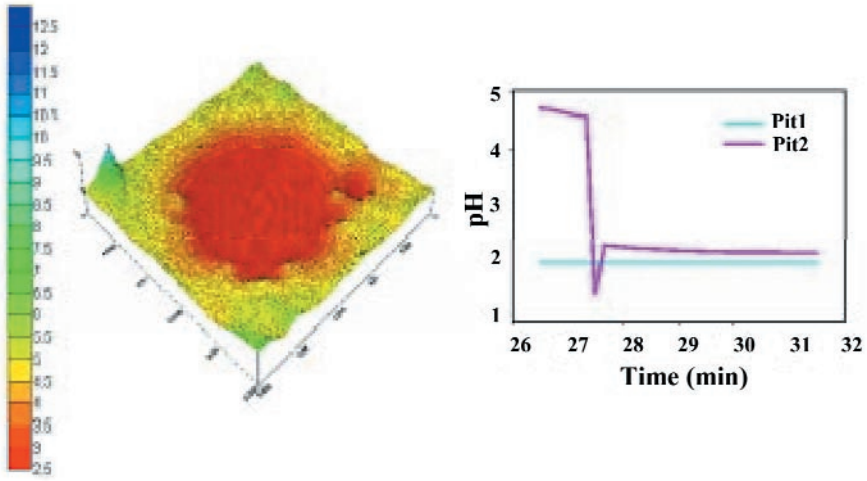

Figure 2. Left: pH map of two pits (pit 1 in center, pit 2 on right). Right: pH evolution of pits vs. time showing stability of pit 2 after initiation at 27.5 minutes. The fact that the pH of pit 2 remains below 3 indicates it is stable.

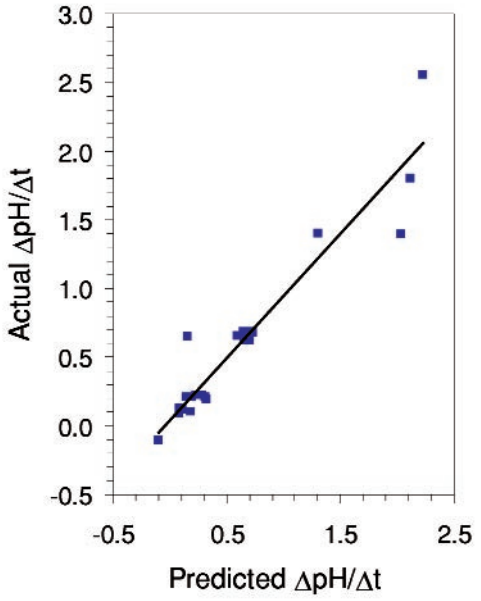

Figure 3. Predicted time-rate of change of pH over the second pit at four minutes vs. actual time-rate of change of pH from computational model.

Characterization of Intermetallic Particle Electrochemistry and Localized Corrosion in High Performance Aluminum Alloys

R. G. Buchheit, R.M. Leard** and **H. Guan
Ohio State University

Motivation—Aluminum alloys derive their excellent mechanical properties from a dispersion of hard microscopic particles formed by alloying and processing. These particles, sometimes referred to as "intermetallics", contain high concentrations of alloying elements such as Cu, Mg, Zn, Mn, Si and Li, which may be added to aluminum in amounts ranging from 0.1 to nearly 10%. Figure 1 shows a scanning electron micrograph from a metallographic polished section of 2024-T3 (Al-4.4Cu-1.5Mg-0.6Mn) that illustrates a typical dispersion of large intermetallic particles in an Al alloy. While this dispersion of particles is essential for enhanced mechanical properties, their electrochemical characteristics differ from the surrounding Al-rich matrix phase leading to increased corrosion susceptibility. We are interested in understanding how intermetallic particle electrochemistry depends on particle size and chemistry, so that this information can be used to design alloys for improved corrosion resistance, and to aid in developing models to predict accumulation of corrosion damage.

Accomplishment—A microelectrochemical cell has been constructed to measure the electrochemical characteristics in high strength Al alloys on a phase-by-phase basis. The "microcell", which consists of a glass capillary drawn to diameter ranging from 1 to 50 μm, is shown in Figure 2. The cell is mounted on the objective carousel of an optical microscope so that it can be precisely positioned enabling electrochemical characteristics to be measured with high spatial resolution. We have characterized the electrochemistry of many of the intermetallic particle phases in 2024-T3 including Al_2CuMg, Al_2Cu, Al_7Cu_2Fe, $Al_{20}Cu_2Mn_3$, and Al_6Mn. We have also measured the behavior of the matrix phase that is free of large intermetallic particles. We have been able to show that in dilute chloride solutions, like those that exist in many service environments, intermetallic particles passivate, but that this passivity breaks down quite easily. In fact, passivity breakdown of the particles is much easier than that of the particle-free matrix phase suggesting that these particles are the weakest link in terms of resistance to the onset of localized corrosion damage. This is illustrated in Figure 3, which shows polarization curves for some of the intermetallic phases present in the alloy, the particle-free matrix, and the bulk alloy. The onset of localized corrosion damage coincides with a sharp break in the curve to the right associated with an increase in current density as indicated by the arrows. The lower the potential at which the break occurs, the lower the resistance to localized corrosion. The particle-free matrix phase is quite resistant to localized corrosion, but the particles are not. More importantly, the pitting potential of the alloy coincides with the breakdown potential of the intermetallics suggesting that the two processes are closely related.

Significance—The common understanding of pitting in Al alloys is that intermetallic particles serve as small local cathodes that induce pitting in the matrix at their periphery. Our ability to separate corrosion characteristics on a phase-by-phase basis shows that pitting may be more closely related to breakdown of the particles themselves than to particle-induced breakdown of the matrix phase. This new understanding can be used to amend mechanistic interpretations of pitting corrosion, which are the foundation for predictive models for alloy corrosion, and to aid in development of more corrosion resistant alloys.

Contact: Rudy Buchheit, Ohio State University
Phone: (614) 292-6085, Fax: (614) 292-9857, Email: buchheit.8@osu.edu

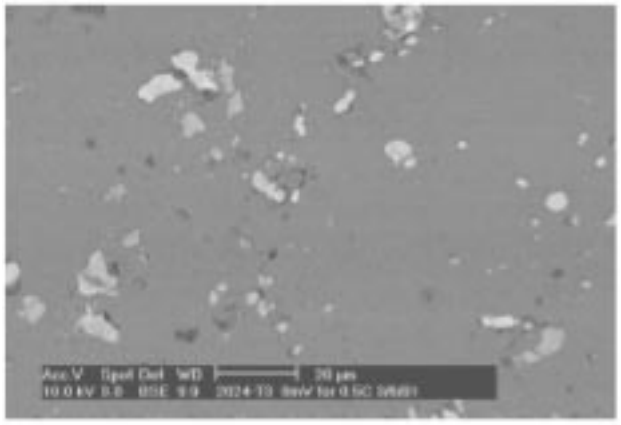

Figure 1. Scanning electron micrograph of a metallographically polished sample of 2024-T3 showing the distribution of intermetallic particles that ultimately contribute to reduced corrosion resistance.

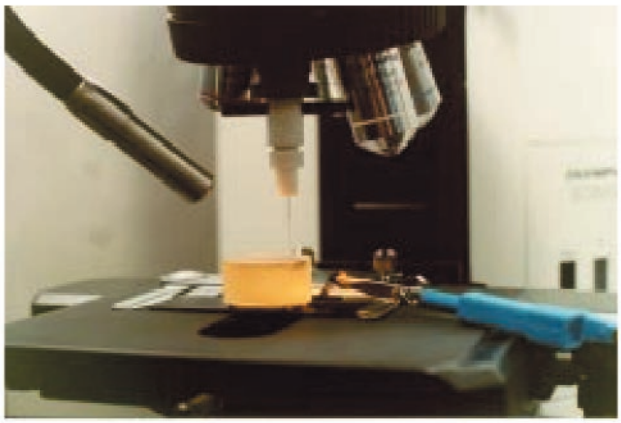

Figure 2. Photograph of the microelectrochemical cell used to measure the electrochemical characteristics of individual phases in a complex microstructure.

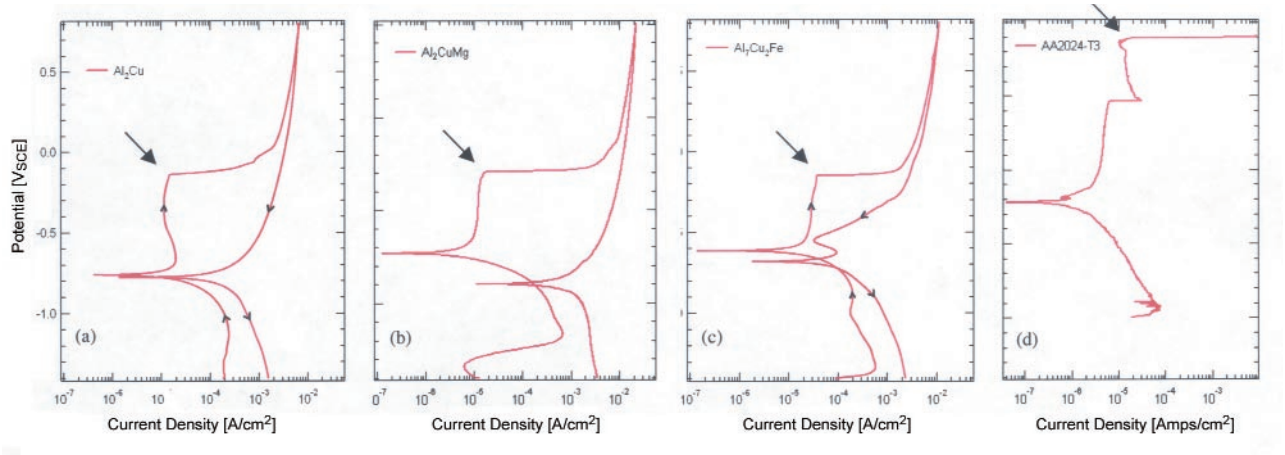

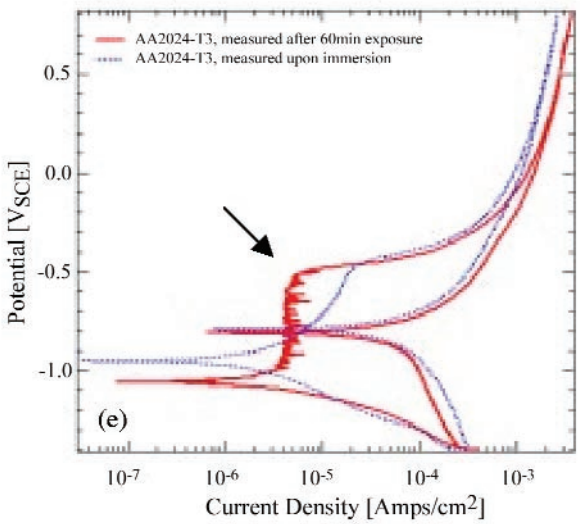

Figure 3. Polarization curves characterize the electrochemical behavior of metals and alloys. This figure shows polarization curves for intermetallic particles: Al_2Cu (a), Al_2CuMg (b), Al_7Cu_2Fe (c), and particle free matrix from 2024-T3 (d). Figure (e) shows the polarization curve for the bulk 2024-T3 alloy that contains all of these phases.

Scanning Electrochemical Microscopy of Electron Transfer at Defect Sites in the Oxide Film on Aluminum and the Relationship to Pitting Corrosion

Irina Serebrennikova and *Henry S. White*
University of Utah

Motivation—The thin oxide film present on the surface of Al is an effective barrier layer that serves to protect the metal against chemical oxidation and dissolution. While exceedingly thin, the ~2.5 nm-thick Al_2O_3 layer is an excellent electrical insulator, greatly reducing the rate of electron transfer between the underlying metal and chemical species in the solution which determines the fundamental rate of corrosion. We are interested in determining if microscopic spatial variations in the electrical conductivity are inherent to the native oxide film on Al and whether or not these variations are related to local breakdown of the oxide film. The initial step in the pitting corrosion of Al is associated with localized breakdown of the passive film, exposing the Al to the environment. Understanding why the oxide film is unstable at a relatively small number of microscopic surface sites is fundamental to a mechanistic description of the pitting corrosion of Al.

Accomplishment—Scanning electrochemical microscopy, SECM, has been developed to image the local electrochemical activity at Al electrodes. SECM is a scanned-probe technique in which a microscopic probe tip is scanned a few micrometers above the substrate surface, Figure 1. The tip amperometrically detects electroactive species generated at the surface as a function of spatial location. The resulting SECM image allows *in-situ* visualization of spatially localized electrochemical activity. When imaging oxide film-covered metals, the redox activity directly reflects the local rate of electron tunneling across the oxide film (for thin films, < 2 nm thick) or the electronic conductivity of the film (for thicker films). For instance, a microscopic redox-active site observed in a SECM image might reflect the higher electronic conductivity associated with a structural (or purely electronic) defect site in an otherwise passive oxide film. Thus, SECM can provide key information on the *local* electronic properties of oxide films that are important in oxide film breakdown and localized corrosion.

Figure 2 shows a SECM image of a small region (300 x 300 μm) of an Al electrode. While most of the Al surface is featureless, the image displays a sharp peak corresponding to a microscopic site where electron transfer across the oxide film is very rapid. From SECM analysis, we estimate the number density of "defect" sites to be ~400/cm^2. Importantly, we have not been able to detect a difference in the chemical composition of these sites of high conductivity, suggesting that they are associated with local differences in physical properties of the oxide film. We are currently investigating the role that these sites play in pitting corrosion. After identifying the positions of the sites of high conductivity, we immerse the electrode in an aqueous chloride solution to initiate pitting corrosion. We have found that many of the sites identified by SECM correspond to the spatial positions of pits (Fig. 3) suggesting that the localized electrical conductivity and oxide stability are closely related.

Significance—Our results are the first to show that a direct link exists between sites of oxide breakdown and local electrical conductivity in the aluminum system. The experimental connection between these two phenomena provides a new experimental and theoretical tool to better understand the mechanism of pitting corrosion. The results suggest that processing methods aimed at reducing the number of electrical defect sites in the oxide film may also lead to improvements in corrosion stability.

Contact: Henry White, University of Utah
Phone: (801) 585-6256, Fax: (801) 585-3207, Email: whit4e@chemistry.utah.edu

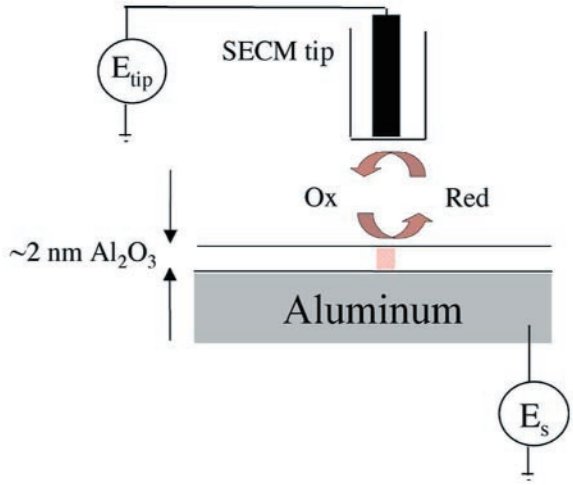

Figure 1. Schematic depicting the SECM measurement of electronic defect sites in the native Al_2O_3 film on an Al substrate. Ox and Red are the electroactive species used to transfer charge between the SECM tip and the Al substrate.

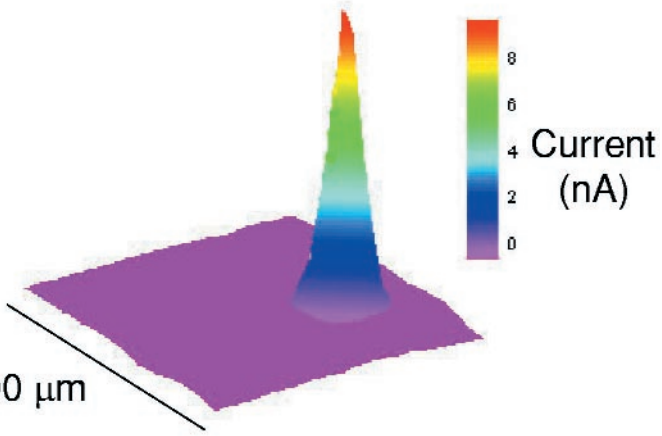

Figure 2. SECM image of a defect in the oxide film on an Al electrode. The signal arises from the high electrical conductivity at the defect relative to the surrounding Al_2O_3 film.

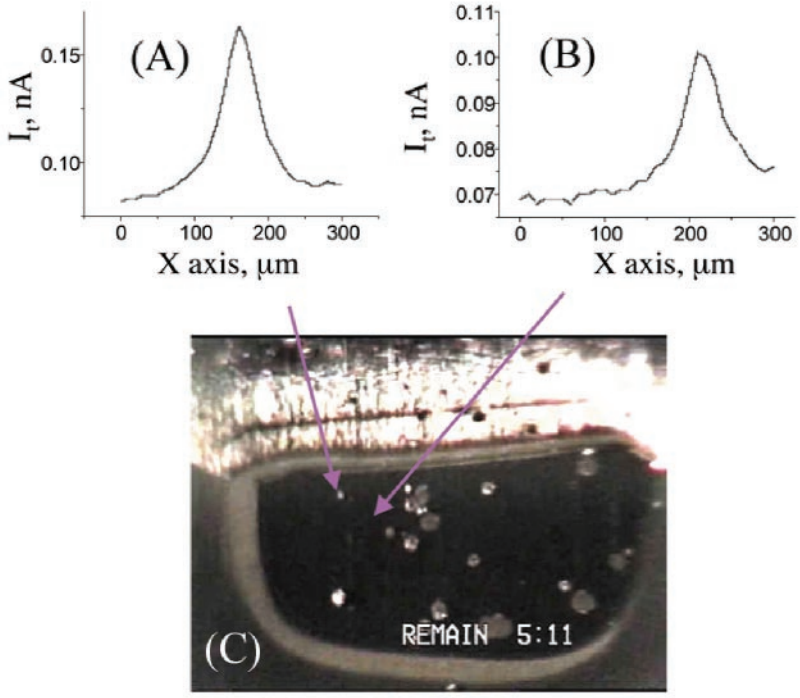

Figure 3. Using SECM to identify precursor sites for oxide film breakdown and corrosion. Figures (A) and (B) show line scans of the SECM tip current measured over different regions of an Al/Al_2O_3 surface, identifying the positions of two conductive defects in the oxide film. Figure (C) shows a photograph of the same sample after allowing the surface to undergo pitting corrosion in a Cl^- solution. The defect site identified in (A) developed into a stable pit (white spot) while the defect site in (B) remained stable. The arrows show the positions of the defects identified by SECM.

Chemical State of Segregants at Al_2O_3-Alloy Interfaces Studied By μXPS at the ALS

P. Y. Hou, Lawrence Berkeley National Laboratory

Motivation—The segregation of solutes and impurities to oxide-metal interfaces is of extreme technological importance. All alloys in high temperature applications rely on an adherent surface oxide layer, or scale, for protection against continued oxidation, but some segregants, particularly sulfur, reduce adherence of this oxide. It is often believed that the reduction is due to a weakening of the interfacial bonds. In order to know how and whether sulfur weakens the metal/oxide interface, its distribution and binding state at the interface need to be evaluated. Scientists at LBNL have pioneered studies of the changes in composition at Al_2O_3-alloy interfaces by debonding the oxide in UHV followed by interfacial examination using Scanning Auger Electron microscopy. Results showed very different amounts of interfacial sulfur on different alloys. Multi-layer segregation and co-segregation of other elements can also occur depending on the alloy composition. Despite these findings, questions on the chemical states of the segregants remain. This information can provide valuable insight into the structure of the interface and how the segregated sulfur may affect interfacial bonding. Since the oxide-alloy interface is buried and large areas cannot be exposed for conventional X-ray Photoelectron Spectroscopy (XPS) analyses, micro XPS (μXPS) at the Advanced Light Source (ALS) was used where the X-ray beam can be focused onto less than 2x2 μm areas.

Accomplishment—Two model alloys were used. One was an iron aluminide, Fe-40Al (at%); the other was Fe-18Cr-10Al (at%) (Figure). It was found that sulfur, chromium and carbon accumulated at Al_2O_3-FeCrAl interfaces, forming a multi-layer that was enriched with chromium sulfide at the surface with underlying chromium carbide. Partial coverage of sulfur was present at Al_2O_3-FeAl interface. While most of the sulfur existed as sulfide, a small portion was present as non-oxidized sulfur, probably due to the strong surface adsorption of oxygen that competed with the sulfur to bind with the metal. Continued adsorption of surface oxygen and carbon did not alter the sulfur binding states on either alloy. These experimental results provide the necessary information to model interfacial bonding and strength. The differences in surface composition and structure reported here for the two iron-based Al_2O_3-forming alloys indicates that there are variations in the interfacial chemistry over and above the sulfur segregation level. These may affect scale adhesion as a second-order, but significant, effect.

Significance—This is the first study on thermally grown oxide-metal interfaces using XPS. The results complement previous AES studies in clearly indicating the differences in interfacial chemistry and structure that can result from different alloy compositions that still form the same surface oxide. Identification of the chemical state of segregants at two Al_2O_3-alloy interfaces provides the necessary information to model interface bonding and strength.

Contact: Peggy Hou, Lawrence Berkeley National Laboratory
Phone: (510) 486-5560, Fax: (510) 486-4995, E-mail: pyhou@lbl.gov

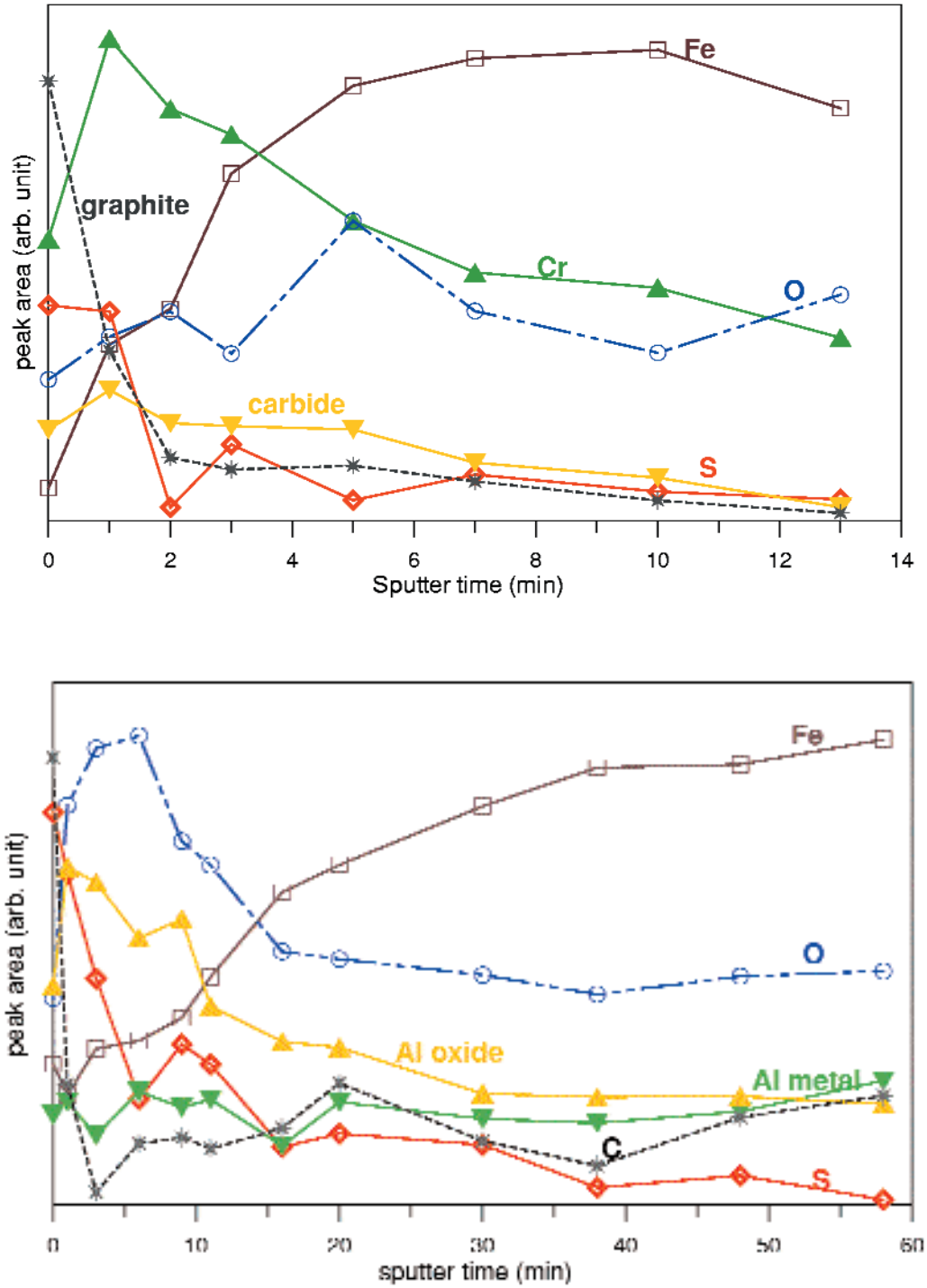

Figure. XPS depth profiles on surfaces of FeCrAl (upper plot) and FeAl (lower plot) after removal of thermally grown Al_2O_3 scale and being held overnight in the $2x10^{-8}$ torr vacuum of the μXPS chamber. On the FeAl, sulfur was the only segregant. Prolonged exposure in the chamber caused surface oxidation forming Al-O. The high concentration of segregants on FeCrAl (S, C and Cr) prevented the formation of such an oxide. On the FeCrAl, the segregants were chromium sulfide and chromium carbide, with the sulfide concentrated closer to the surface.

Measurement of Growth Stress In Chromia

B.W. Veal, A.P. Paulikas and M. Grimsditch
Argonne National Laboratory

Motivation—Thermally grown protective oxides are essential for the successful operation of many high-temperature energy systems, such as turbines. However, there has been, and continues to be, substantial uncertainty regarding the adhesion of these oxides to their metallic substrates and the mechanisms by which decohesion takes place. The development of strains in these films obviously plays an important role in setting the energetics of the oxide-metal system and determining overall adherence. In-situ measurements of strain in such films can help foster a much better understanding of the time-dependence of stress generation and relaxation in these systems and help develop and evaluate appropriate oxide growth mechanisms. These, in turn, are a necessary component of modeling the processes that could lead to debonding at oxide-metal interfaces.

Accomplishment—In-situ high-temperature, growth strains that develop in protective surface oxides as oxidation proceeds have been measured. (From these strains, stresses can be deduced.) The results are coupled with measurements of residual strains resulting from thermal expansion differences between substrate and oxide as determined by ruby fluorescence spectroscopy.

X-ray diffraction measurements of growth strains were made using undulator radiation and a special environmental chamber at the Advanced Photon Source. Diffraction patterns of the polycrystalline (Fe-Ni-Cr) metal alloy, and of the overlying growing chromia, were simultaneously recorded during oxidation at 720°C. The known lattice parameters of the substrate alloy were used as an internal calibration to accurately determine the strain state of the growing oxide. For the [116] plane of Cr_2O_3, d-spacings were obtained from in-plane and out-of-plane measurements (Figure). The data indicated that a 0.26% in-plane compressive strain has developed during oxidation at 720°C. With in-plane compression, the free surface of the oxide expands in accordance with the Poisson ratio, or about 0.13%.

Significance—The rapid and detailed determination of strain evolution in thin protective oxides is achievable only with the use of synchrotron radiation. These initial data illustrate the utility of synchrotron sources for this type of measurement. The present finding of a substantial at-temperature strain in this system indicates that the oxide growth process is an important source of stress in at least some protective oxide systems.

Contact: Boyd Veal, Argonne National Laboratory
Phone: (630) 252-4957, Fax: (630) 252-7777, E-mail: veal@anl.gov

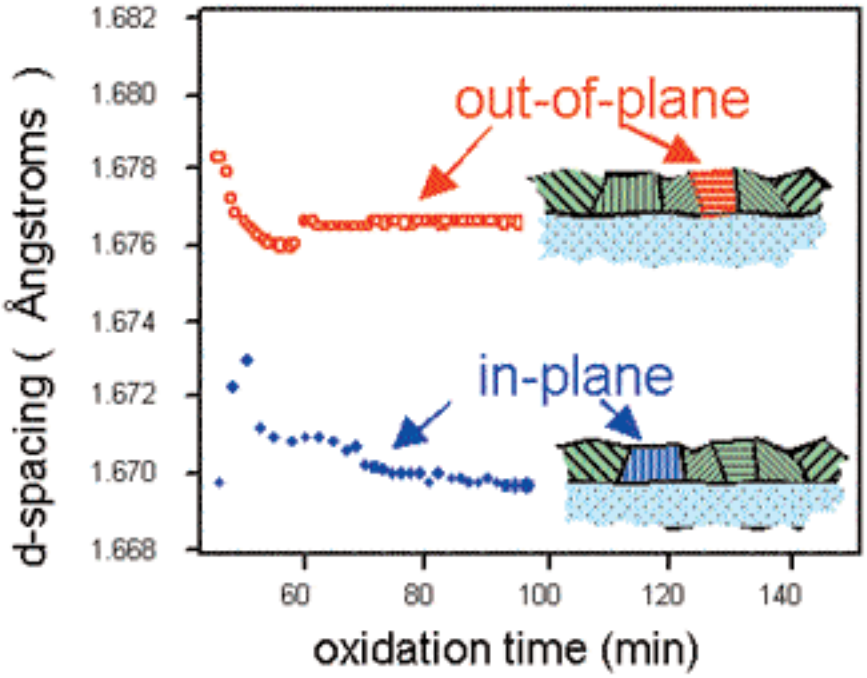

Figure. Lattice parameter data obtained from the surface of an Fe-Ni-Cr alloy undergoing oxidation at 720°C using synchrotron radiation. At longer times, a fairly constant 0.26% in-plane compressive strain in the chromia was measured. With in-plane compression, the free surface of the scale expanded in accordance with the Poisson ratio, or about 0.13%.

Computational Investigation of Crack Propagation in Oxide Films and Coatings

R. L. Williamson *and* ***J. K. Wright,*** *Idaho National Engineering and Environmental Laboratory*
R. M. Cannon *and* ***P. Y. Hou,*** *Lawrence Berkeley Laboratory*

Motivation—Regions of local curvature in coatings or oxide films, due either to corners or convolution of the substrate surface, can develop significant tensile stresses and stress gradients during changes in temperature. For cooling of an oxide on a metal substrate, the largest tensile stress component is typically within the outer portion of the film and in a direction normal to its surface, leading to concerns about cracking. Localized curvature also results in tensile stress in the substrate near the material interface, and, since the main tensile component is in a direction parallel to the interface, interfacial cracking or decohesion is of interest. Both types of failure are observed in oxidation studies. The objective of this research is to computationally investigate fracture behavior in regions of local curvature to better understand failure mechanisms, and, ultimately, to provide criteria for design of more adherent oxide films or coatings.

Accomplishment—Finite element continuum models were developed to analyze surface and interface cracking at regions of local curvature in oxidized specimens during cooling from a stress-free condition at 1000°C to ambient temperature (Figure). The geometry considered is essentially a square cross section metal rod covered with a uniformly thick oxide film. The corners of the rod are rounded and contain either a surface crack perpendicular to the oxide-substrate interface or an interfacial crack. Material properties typical of Al_2O_3 and Fe_3Al were used for the surface oxide and substrate, respectively. Crack motion was simulated using a series of standard static fracture analyses with varying crack lengths, assuming a crack propagation direction. This approach permits very fine meshing near the crack tip, providing detailed stress/strain fields in this region. Additionally, an accurate numerical approximation of the stress intensity factor is possible for comparison to measured fracture toughness data.

Surface crack calculations demonstrate that for certain geometric conditions and material properties, the stress-intensity factor exceeds the fracture toughness in the oxide, indicating potential for crack growth. Sharper corners and lower substrate yield strengths increase the growth potential. Interestingly, the constraining effects of the substrate eventually cause a reduction in the stress-intensity factor with increasing crack length, leading to crack arrest or turning. Stress fields in the vicinity of the crack tip suggest that, rather than arrest, a surface crack will turn back toward the free surface of the oxide.

Interface crack simulations show a clear shift in fracture behavior from Mode I (tensile) to Mode II (shear) during crack growth. Interface cracking results in substantial increases in the normal stress on the oxide surface, thus free surface and interface cracks are undoubtedly coupled.

Significance—Several factors make it difficult to analyze crack behavior in regions of curvature. The stress field where cracks initiate and propagate is strongly dependent upon local geometry, temperature changes, nonlinear material behavior, substrate constraint, and relief due to crack motion. Multiple cracks are possible. In some cases, these complexities have resulted in unexpected results. Computational models have led to a significantly improved understanding of failure mechanisms and local fracture behavior.

Contact: Rich Williamson, Idaho National Engineering and Environmental Laboratory
Phone: (208) 526-0576, Fax: (208) 526-0690, E-mail: rlw@inel.go

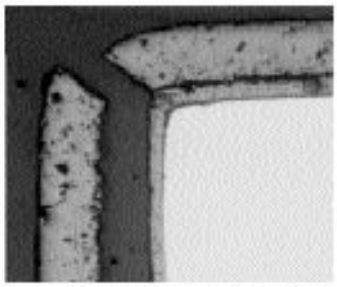

a) Typical cracking pattern at corner

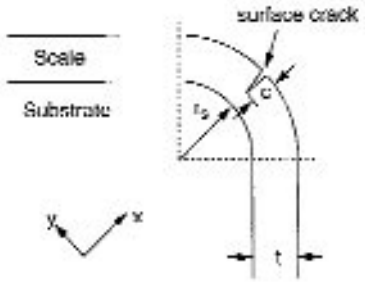

b) Schematic of surface crack at corner

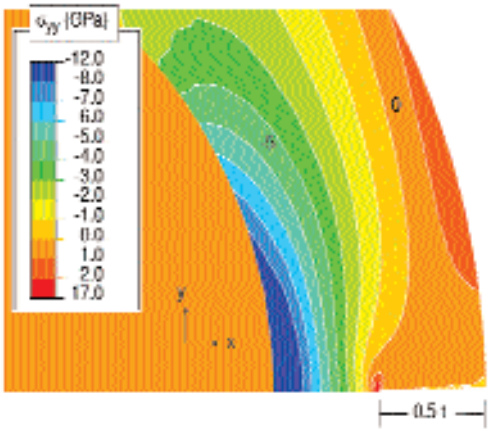

c) Contour plot of σ_{yy} in the vicinity of a surface crack through half the scale thickness

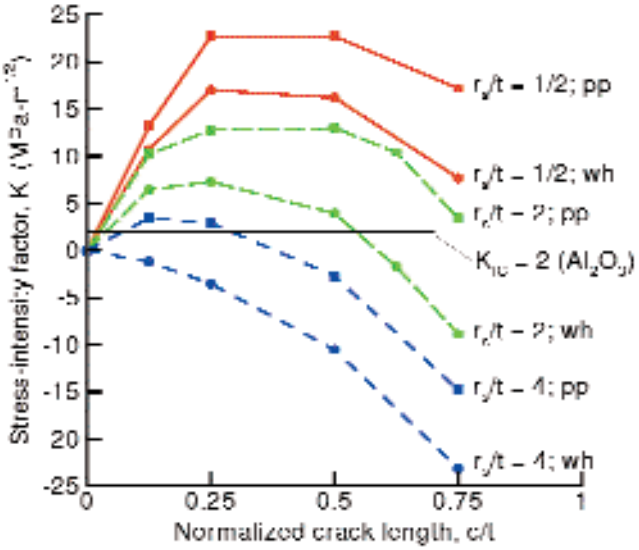

d) Stress intensity factor as a function of surface crack length for various conditions (pp - perfectly plastic, wh - work hardening substrate)

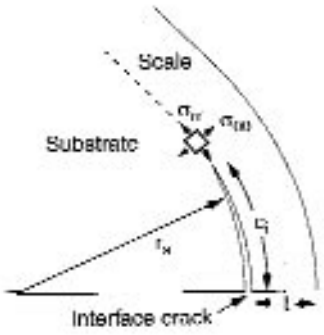

e) schematic of interface crack

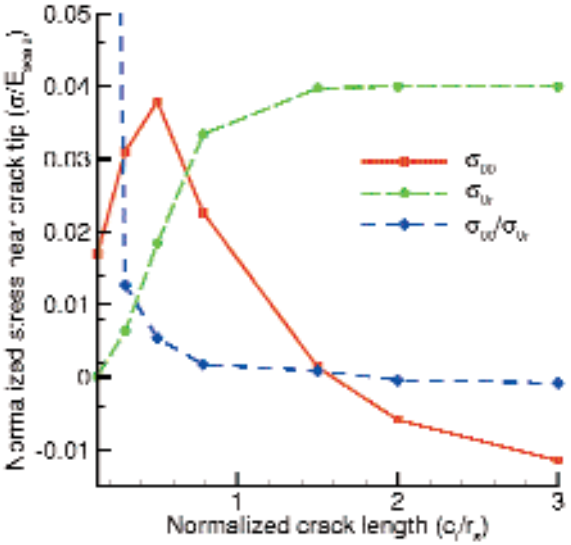

f) Crack tip stress as a function of interface crack length

Figure - Cracking at corners in oxide films and coatings (a) has been investigated using a variety of finite element models. For surface cracks (b), tensile stresses and stress gradients in the oxide (c) lead to potential crack growth ($K>K_{IC}$) (d), however large stress gradients (c) can cause the cracks to arrest or turn. Interface crack models (e) show a clear shift from Mode I to Mode II behavior during growth (f).

The Role of N Isoelectronic Traps in GaInAs

A. Mascarenhas[1], E.D. Jones [2], C.W. Tu[3] , V. Narayanamurti[4],
W. Wlalukiewicz[5] and D.J. Wolford[6]
[1]NREL, [2]SNL, [3]UCSD, [4]Harvard, [5]LBL, [6]Iowa State Univ

Motivation—To achieve solar cell efficiencies > 40%, it is necessary to add a fourth absorbing semiconductor layer to the current state-of art three-junction solar cell comprising Ge, GaAs, and GaInP, where this fourth layer optimally has a bandgap close to 1 eV and is lattice matched to GaAs. Hitherto it was impossible to obtain such a material using any alloy combination from the available repertoire of III-V semiconductors. However, it was recently found that GaInAsN with a few percent of nitrogen has the desired bandgap and lattice constant. Although there was initial excitement that GaInAsN would be the ideal 1eV absorber, it soon became evident that it's electron lifetime, mobility and diffusion length were severely degraded with respect to GaAs, thus resulting in poor photovoltaic performance. It is thus necessary to determine the origin of these limitations.

Accomplishment—Since N is insoluble in GaAs, it is incorporated using non-equilibrium growth techniques which inevitably result in a small fraction of interstitial N and consequently the generation of traps that lower the radiative recombination efficiency. Post growth annealing of the samples results in removal of the interstitial N and elimination of the trap states. In spite of this, the carrier lifetime, and electron mobility remain quite low indicating that these parameters are intrinsically limited in dilute GaAsN. Since the carrier lifetimes are short it has not been possible to measure the conduction band effective mass, m_e, using cyclotron resonance techniques. We therefore measured m_e by synthesizing quantum wells of GaAs barriers and GaAsN wells with varying well widths and N concentrations. By determining the confinement-induced shifts of the ground and excited states as measured by electroreflectance techniques, the variation in m_e with N composition was obtained. As Fig. 1 indicates, at low N concentrations m_e is almost an order of magnitude higher than that for GaAs and as the N concentration is increased this value gradually approaches that of GaAs. This kind of unusual behavior is typical of impurity bands and hints at an alternative explanation to the level repulsion models for the giant bandgap bowing in GaAsN. In this aternative view, the formation of impurity bands from interactions between the isoelectronic N impurity levels gives rise to the bandgap lowering quite analogous to that observed conventionally in heavily doped semiconductors such as GaAs:Si. Nitrogen, unlike phosphorous, is isoelectronic with As, and GaAsN can be viewed as an alloy rather than as a heavily doped semiconductor. In contrast to conventional dilute alloys, e.g., GaAsIn, for which In does not generate bound states, N generates bound states (the NN traps) and thus exhibits behavior that resembles GaAs:Si rather than GaAsIn. This is best illustrated by a scaling shown in Fig.2. The change in slopes from 1/3 to 2/3 between GaAs:Si and GaAsN is due to the fact that impurity band formation is dominated by interactions between impurity pairs in the former and isolated impurities in the latter.

Significance—It is important to determine whether the limitations of the dilute GaAsN and GaInAsN are due to intrinsic or extrinsic factors and whether it is possible to overcome them. The present results are a first step in this quest and shed new light on the unusual bandgap bowing, its underlying mechanisms and provide a new perspective on substitutional alloys.

Contact: Satyen Deb, National Renewable Energy Laboratory
Phone: 303-384-6405, Fax: 303-384-6481, E-mail: satyen_deb@nrel.gov

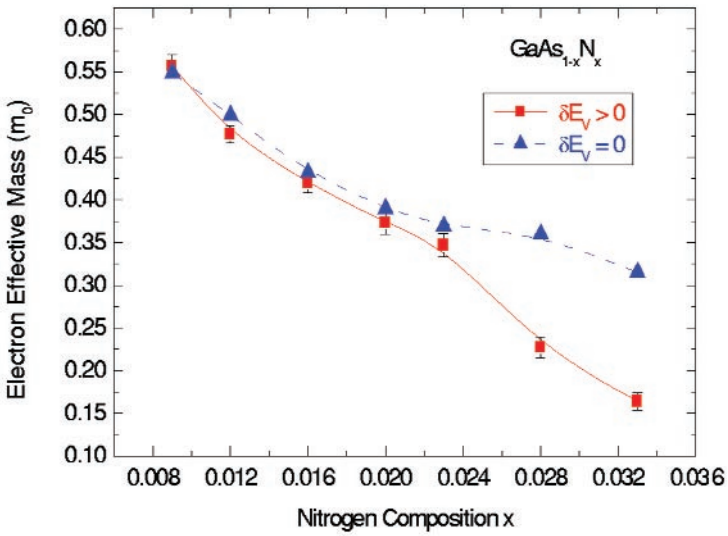

Figure 1. Electron effective mass vs Nitrogen content.

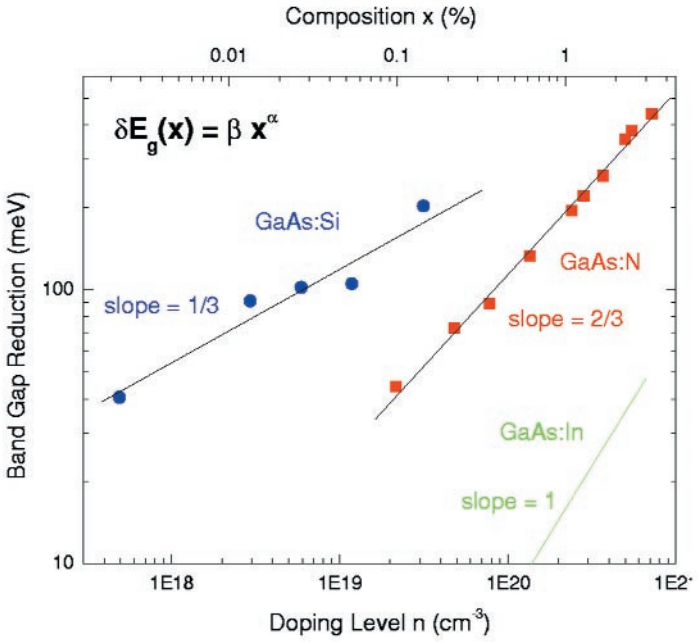

Figure 2. Scaling of the band gap reduction.

Thin Si Films for Low-Cost Solar Cells

R. Aparicio and R. Birkmire, *University of Delaware*
B. L. Sopori, *National Renewable Energy Laboratory*
A. Rohatgi, *Georgia Institute of Technology*

Motivation—The need to reduce manufacturing costs of crystalline (c)-Si wafer-based photovoltaics has attracted significant interest in thin film silicon technologies. By combining large area monolithic integration on low cost substrates and improved manufacturability, thin film Si can become a lower cost alternative to c-Si. In theory, thin Si solar cells have also the potential to exceed the efficiency of thick Si solar cells due to reduced volume recombination, provided that successful light trapping and surface passivation can be achieved. However, several critical issues must be resolved before thin film silicon can replace c-Si. Needed is a fast and efficient Si thin film fabrication processes at low substrate temperatures (<600° C). Hot-Wire Chemical Vapor Deposition (HWCVD) can meet these requirements. However, HWCVD Si films always have a grain size of 10-50 nm. To obtained desired photovoltaic efficiency, its has been postulated that the grain size should approach values equivalent to the film thickness, which is expected to be in the range of 2-10 micrometers for effective light absorption with light trapping. Therefore, our research in this Center project has focused on the development of the HWCVD process in conjunction with low temperature grain enhancement techniques that produce micrometer sized Si grains.

Accomplishment—At the Institute of Energy Conversion, University of Delaware the HWCVD process is being developed to meet the requirements for thin film Si (figure 1). We have demonstrated polycrystalline Si film depositions at substrate temperatures as low as 300 °C, with film growth rates and reactant conversions as high as 10 μm/hr and 90%, respectively (figure 2-4). P-type doping has also been achieved, with film resistivities varying from 10^{-2} to 10^{2} ohm-cm. To solve the problems associated with small grain size, collaborations have been established with Dr. B. Sopori (NREL) and Prof. A. Rohatgi (Georgia Tech - GIT). Both of these groups are investigating the use of post-deposition techniques for grain size enhancement. At GIT, Rohatgi is developing a metal-induced crystallization (MIC) process which uses rapid thermal annealing. IEC has supplied both amorphous and poly-crystalline films to this group to assess the feasibility of this approach. One of Rohatgi's students has also visited IEC and assisted in the deposition of Si films. At NREL, Sopori is investigating the process of optically assisted metal-induced crystallization. His group visited IEC and participated in the deposition of various samples. The films were then processed for grain enhancement at NREL. Figure 5 shows the crystallization front that develops from the interaction of the as-deposited Si film and the Al metal layer. After 3 min of optical processing at 460 °C, 0.1 μm grains can be observed on the TEM image. Since the film was only partially crystallized, it is expected that longer processing times and complete crystallization will lead to an even larger grain structure.

Significance—HWCVD combined with post-deposition MIC is a promising approach to develop thin Si film solar cells. The fast growth rates, high conversions and low temperature deposition on glass are important ingredients to achieve manufacturing cost reductions. With the successful development of grain enhancement, impurity control and light trapping approaches to address performance issues, thin film Si can become a cheaper, high performance alternative

Contact: Satyen Deb, National Renewable Energy Laboratory
Phone: 303-384-6405, Fax: 303-384-6481, E-mail: satyen_deb@nrel.gov

Figure 1. HWCVD reactor system at IEC

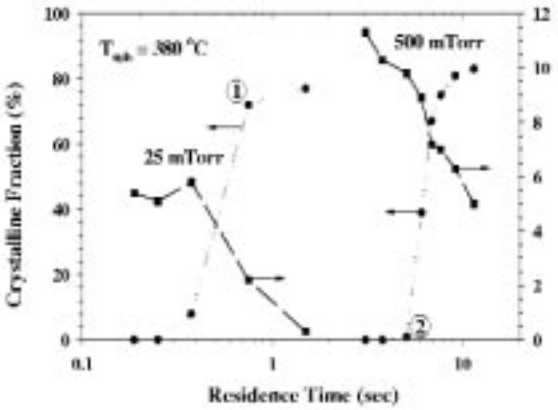

Figure 2. Effect of residence time on the growth rate and crystalline fraction of HWCVD films.

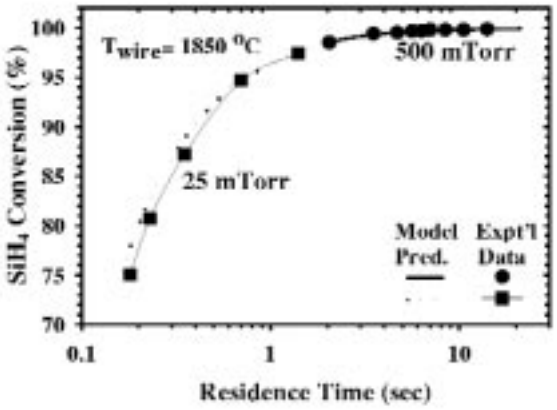

Figure 3. Effect of residence time on the conversion of silane in HWCVD.

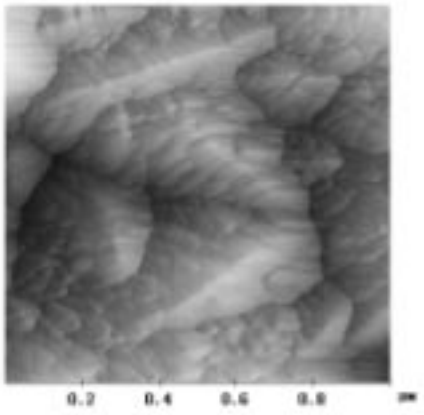

Figure 4. Grain Structure of as deposited HWCVD films.

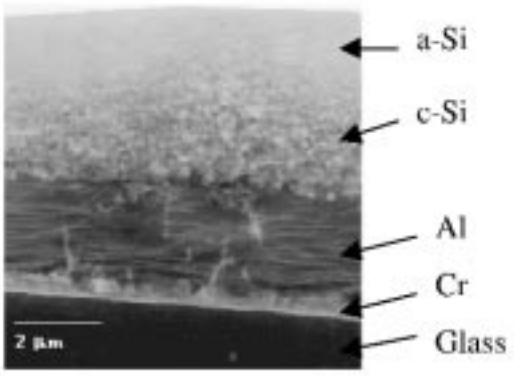

Figure 5. TEM photos of a partially crystallized Si film showing start of nucleation and grain growth from the Al interface in cross section (left) and grain size distribution in plan view (right).

Resonance Ultrasonic Diagnostics of Stress Induced Defects in EFG mc-Si

I. Tarasov, A. Belyaev, S. Lulu *and* ***S. Ostapenko,*** *University of South Florida*
J. P. Kalejs, *ASE Americas*

Motivation—Thermo-elastic stress in Edge-defined, Film-fed Growth (EFG) microcrystalline silicon (mc-Si) wafers can be generated during crystal growth and following cooling phase. The stress depends upon sheet growth velocity, its thickness, and temperature distribution. If sufficiently large, the thermo-elastic stress creates wafer buckling, dislocations and permanent plastic deformation. Additional stress related problems are created by laser cutting techniques when edges of the wafers are damaged due to laser processing. Laser processing creates favorable conditions for micro-cracks leading to wafer fracture and breakage. Finding an express reliable method to control residual stress and micro-cracks in EFG materials and development of on-line methodology to eliminate potentially bad wafers from the production of devices are high priority goals. As one of the coordinated research activities in this Cener project, we have developed a new experimental approach based on resonance ultrasonic vibrations of full-size silicon wafers. The method is promising for Si quality assurance for photovoltaics as well as ICs.

Accomplishment—Ultrasonic vibrations are generated in the wafer using broad band piezoelectric transducer, which is pressed by vacuum against the back-side of the wafer, as shown in Figure 1. This geometry of acoustic loading offers reliable acoustic coupling and a rapid change of sample. A function generator and a power amplifier provide an *ac* driving voltage to the transducer with a tunable frequency (*f*) and adjustable amplitude (*a*). The system is computer controlled and operates with Windows-based software. An air-coupled ultrasonic probe is positioned above the wafer and measures with high accuracy the amplitude of the standing waves generated in the wafer. The probe is attached to the moving stage and creates in a mapping mode the acoustic image of the vibrating wafer. We applied the technique to a commercial set of 10 as-grown 4"x4" EFG wafers. The wafers had different values of in-plane stress ranging from 4.1 to 9.3 MPa measured using a scanning linear polariscopy technique at our lab. All wafers were studied with the resonance acoustic technique. The amplitude of the wafer vibrations and the full width, Δf, of the resonance curve were measured at four symmetrical locations of the probe above the wafer. The result are shown in Figure 2. There is a clear trend in the Δf versus stress dependence. Detail studies of the resonance response of wafers of different processing histories are in progress.

Significance—The resonance acoustic technique has a potential to provide on-line quality control of mc-Si wafers at different processing steps. It is designed as a "snap-shot" method compatible with high-throughput processing environments of mc-Si solar cells.

Contact: Satyen Deb, National Renewable Energy Laboratory
Phone: 303-384-6405, Fax: 303-384-6481, E-mail: satyen_deb@nrel.gov

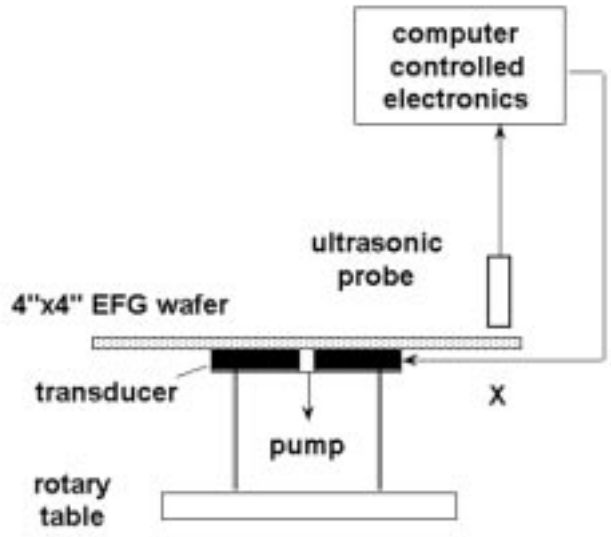

Figure 1. A schematic of computer controlled set-up for non-contact monitoring of ultrasonic vibrations in EFG wafers.

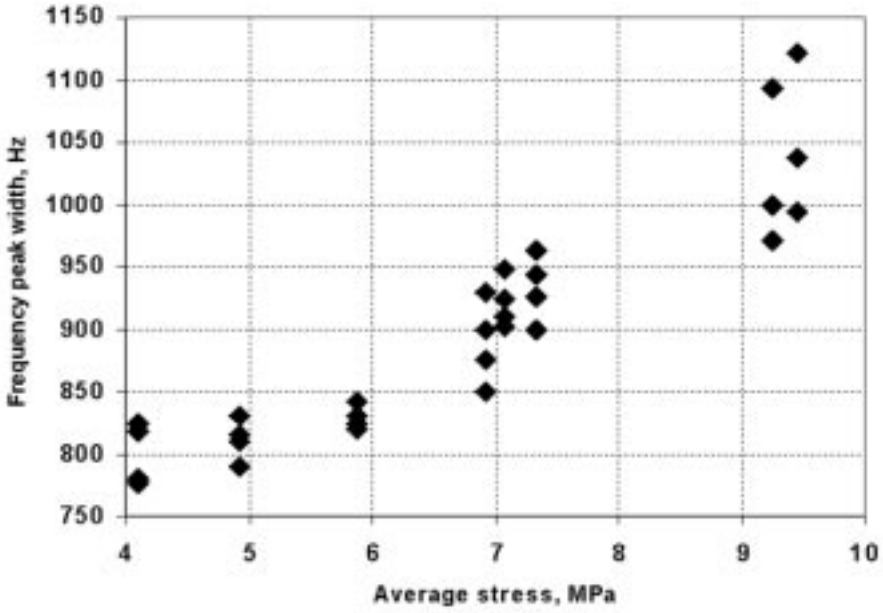

Figure 2. The width of the frequency peak increases with the average stress value in the set of as-grown 4x4" EFG wafers. Every wafer was measured in four orthogonal symmetrical spots in the middle of square sides 1 mm from the edge.

Mechanism of Epitaxial Growth of $YBa_2Cu_3O_7$ for Advanced Superconducting Wires

M. Suenaga, *Brookhaven National Laboratory*
M. Siegal, *Sandia National Laboratory*

Motivation—Electrical conductors utilizing polycrystalline $YBa_2Cu_3O_7$ (YBCO), a high temperature superconductor, are expected to replace Cu cables for future electric power systems because of their high current-carrying capabilities. However, in order to realize this expectation, YBCO, which has an orthorhombic crystal structure with crystal axes *a, b,* and *c,* must be fabricated as highly textured films on long thin metallic tapes with the *c*-axis perpendicular to the tape plane and near perfect *a* and *b* axes alignment in-plane. The necessity for the texture is because grain boundaries in the superconductor are incapable of transporting useful currents unless adjacent grains are aligned within a few degrees. The method of producing such tapes must be capable of fabricating km lengths in short times. The so-call BaF_2 process, a post-deposition reaction process, for the synthesis of YBCO has potential to be cost effective for such applications. The key to success for this method is learning how to grow epitaxial, thick YBCO layers from a precursor film on a bi-axially oriented oxide substrate. The understanding of the process of textured nucleation is of primary importance in this process.

Accomplishment—A combination of reaction kinetics studies and transmission electron microscopy has revealed key aspects of the nucleation process. The nucleation is found to be assisted by the alignment of the (111) plane of an intermediate reaction compound to the (100) plane of the substrate, $SrTiO_3$. This alignment reduces the kinetic barrier for the formation of YBCO from the precursor mixture. The BaF_2 process for the formation of YBCO consists of deposition of a precursor film, a mixture of Y, Cu and BaF_2, on a substrate by evaporation or sol gel methods and heating it in an atmosphere containing H_2O and O_2 in N_2 as shown schematically in Fig. 1. The keys to understanding this epitaxial nucleation process are two fold: (1) the discovery of a newly identified intermediate reaction compound, an (Y,Ba)-oxy-fluoride, which has a very strong chemical affinity to $SrTiO_3$ and segregates to the $SrTiO_3$ surface at the beginning of heat treatment as shown in Fig. 2-A; and (2) the hetero-epitaxial alignment of its (111) planes with the (100) plane of $SrTiO_3$ as shown in Fig. 2-B. Upon further heating, YBCO nuclei form from the interface between the oxy-fluoride and $SrTiO_3$ assisted by this alignment. As a result a kinetic barrier against YBCO formation is lowered by the epitaxial alignment of the oxy-fluoride's (111) plane at the $SrTiO_3$ surface making possible the formation of epitaxial YBCO nuclei resulting a *c*-axis oriented YBCO film with good *a-b* alignment.

Significance—The capacity to carry large currents (high I_c) is perhaps the most important property for electric power applications of YBCO conductors. Although thin film tapes (< 2μm) have been made with high current capacity per unit area, the needed high current requires films thicker than 5 μm. Previously, the formation of such thick films caused substantial amounts of misoriented ("non-*c*-axis") grains, which degrade I_c. The new understanding of the mechanism of *a-b* textured *c*-axis YBCO nucleation, will help to modify the BaF_2 process to avoid nucleation of misoriented grains.

Contact: Masaki Suenaga, Brookhaven National Laboratory
Phone: (631) 344-3518, Fax: (631) 344-4071, E-mail: mas@bnl.gov

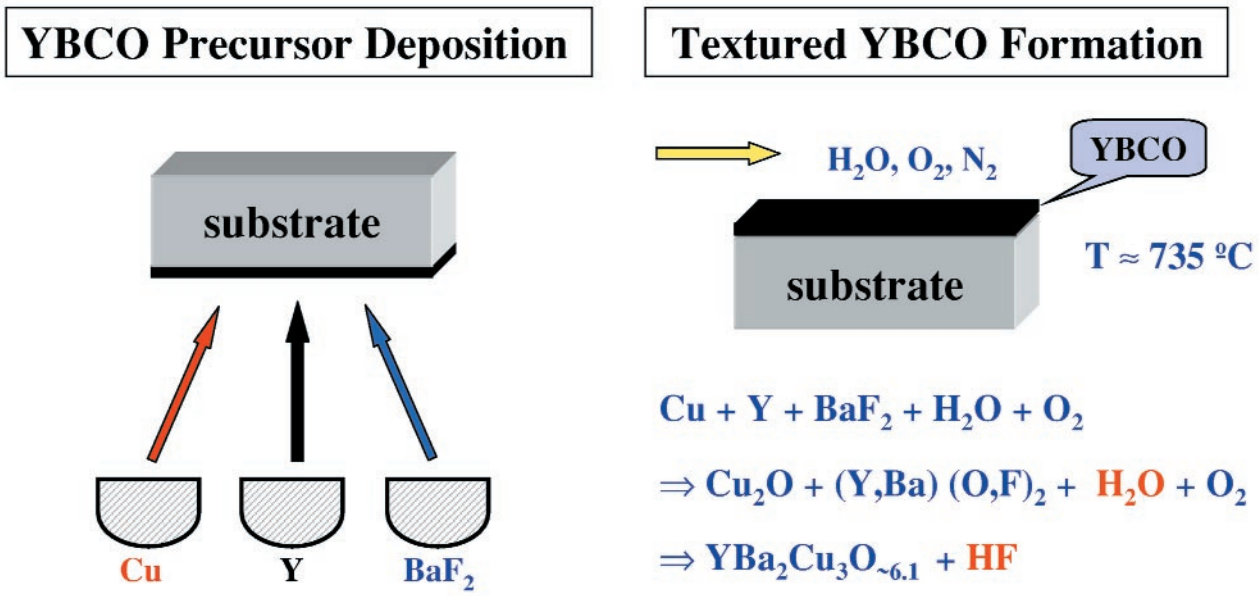

Figure 1. Schematic diagrams for the BaF_2 process for the deposition and chemical reaction of YBCO thick films on the substrates.

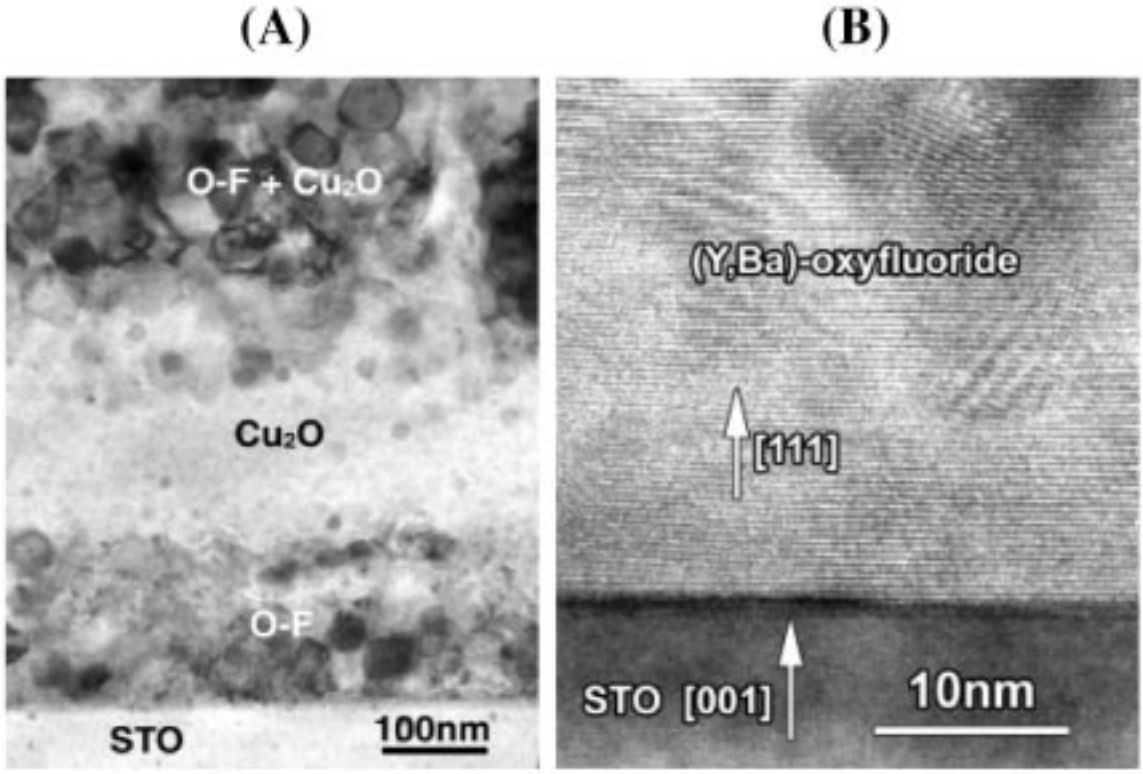

Figure 2. Cross sectional transmission electron micrographs illustrating (A) the segregation of precursor (Y,Ba)-oxy-fluoride to the $SrTiO_3$ substrate surface and (B) the alignment of the (111) plane of the oxy-fluoride on to the (100) plane of $SrTiO_3$, resulting in biaxially textured, c-axis nucleation.

Strontium Doping of Grain Boundaries in YBCO for Improved Current Transport

B. W. Veal, A. P. Paulikas, H. Claus, L. Chen *and* ***K. E. Gray***
Argonne National Laboratory

Motivation—$YBa_2Cu_3O_{7-\delta}$ (YBCO) is expected to play a major role in electrical transmission, generation and utilization. Transport properties of YBCO are outstanding, but there are formidable processing challenges. Highly textured films must be fabricated on metallic tapes such that a high degree of crystallographic alignment is maintained within the YBCO structure. Grain boundaries are incapable of transporting useful currents without such alignment. However, it has recently been shown that calcium doping of YBCO grain boundaries yields impressive improvements in supercurrent transport offering the possibility that the requirement for a high level of texture might be relaxed, greatly simplifying tape fabrication. Unfortunately, Ca poisons bulk YBCO by reducing its superconducting transition temperature (T_c), potentially limiting its use at 77 K, using liquid nitrogen as refrigerant. The mechanism by which Ca improves grain boundary transport is incompletely known. A significant challenge, is to develop a method to minimize the deleterious effect of grain boundaries without impairing performance at 77 K.

Accomplishment—We have found that Sr doping of YBCO grain boundaries yields a factor of 3 to 5 times improvement in critical current, similar to gains achieved with Ca doping, *but without any reduction in* T_c. Transport was studied in bicrystal [001] tilt GBs, made by dual-top-seeded melt-textured growth, and in untextured polycrystalline ceramics. After initial transport measurements, samples were immersed in a $SrCO_3$ powder in an alumina crucible and were heated at temperatures of 930-970 °C for up to 60 hours resulting in Sr diffusion into the GBs. Critical current density J_c(T) results are shown in Fig. 1. At 84 K, Sr-doping yields an improvement of almost a factor of 5 in J_c. Similarly, measurements on ceramic YBCO yield a factor of ~3 increase in J_c at 80 K (Fig. 2). These results are very similar to those we observed for Ca doped GBs, but improvements with Ca doping occurred *at lower temperatures*, i.e., below 77 K. While the problem associated with the reduction of T_c with Ca doping in films has apparently been mitigated with a complex multilayer fabrication approach, doping with Sr offers the promise of greater simplicity. Further, the Sr study provides new insight into the mechanism by which GB dopants enhance J_c. In bulk YBCO, Ca^{2+} is known to substitute for Y^{3+}, increasing the (electron) hole concentration. Similarly, Ca doping of GBs is thought to increase the hole concentration, compensating for an intrinsic depletion of hole carriers at grain boundaries. However, Sr^{2+} substitutes for Ba^{2+} in bulk YBCO, thus simple valence arguments do not indicate that significant hole compensation will occur. We propose that the relevant mechanism is the incorporation of dopant atoms into the dislocation cores of grain boundaries to reduce the intrinsic tensile strain, which, according to theory, will diminish the hole depletion.

Significance—Doping GBs with Sr has significant implications for thin-film coated conductors and for textured bulk materials that will operate close to T_c. Excess Sr could potentially be incorporated directly in coated conductor films to provide desired grain boundary doping and enhanced J_c, without significantly affecting the bulk T_c. The results also give new insight into the *mechanism of grain-boundary transport* suggesting that *substitution in the YBCO structure* (to increase carrier concentration) does not play a dominant role, as previously assumed, but local strains do.

Contact: Boyd Veal, Argonne National Laboratory
Phone: (630) 252-4957, Fax: (630) 252-7777, E-mail: veal@anl.gov

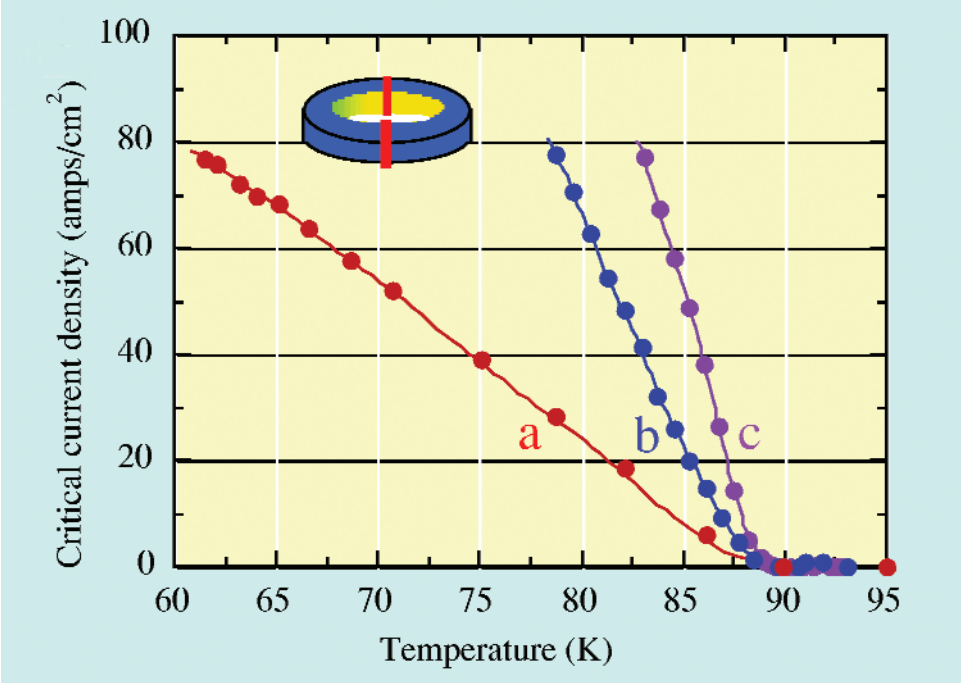

Figure 1. Curve a: J_c vs temperature, measured across a 29° [001] tilt grain boundary. Curve b: J_c(T) after the sample was treated in $SrCO_3$ powder, for 60 hrs at 970 C, to dope the grain boundary with Sr. Curve c: J_c(T) after an additional heat treatment at 930 C.

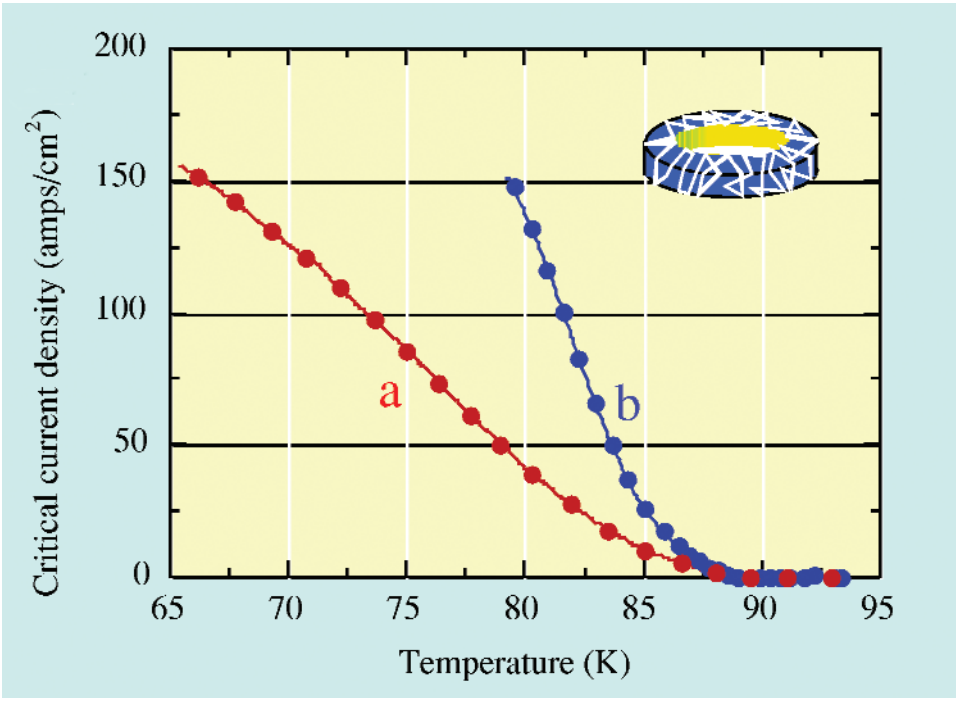

Figure 2. Curve a: J_c(T), for a polycrystalline ceramic sample. Curve b: J_c(T) after the sample was treated in $SrCO_3$ powder to dope the grain boundaries with Sr. Sr doping shows a significant enhancement in J_c without depression of T_c.

Improved Properties of $Hg_1Ba_2Ca_1Cu_2O_x$ for Possible Coated Conductor Applications

D. K. Christen, *Oak Ridge National Laboratory*
D. J. Miller, *Argonne National Laboratory*
J. Z. Wu, *University of Kansas*

Motivation—The next generation of superconducting wires is under development using the "coated conductor" approach, where long lengths of highly grain-oriented HTS coatings are epitaxially deposited on metal tapes. This approach is key to overcoming the problem of "weak-link" current transport across high-angle grain boundaries in cuprate superconductors. The preferred HTS coating material has been $YBa_2Cu_3O_7$, because of its low electronic anisotropy, and therefore excellent flux pinning properties at high magnetic fields and temperatures. Among the obstacles to development of YBCO coatings are difficulties in maintaining high critical current densities in processed thick coatings (> 2 μm, needed for high currents), and in developing appropriate high-rate deposition techniques. While alternative HTS coatings have received little attention due to their inferior flux pinning, for some applications there could be clear advantages for materials that are more easily processed, yet still maintain useful properties. We have investigated the feasibility of developing a Hg-based HTS for this purpose.

Accomplishment—A new fabrication approach has been used to produce 3 μm thick, high-quality coatings of $HgBa_2Ca_1Cu_2O_x$ (Hg-1212), and experiments to introduce controlled flux-pinning defects have shown significant enhancements in the electrical transport properties. The synthesis is accomplished in three steps: a Tl-rich precursor coating of $Tl_2Ba_2Ca_1Cu_2O_x$ was deposited, followed by an *ex situ* heat treatment to form high-quality, superconducting Tl-2212. In a final heat treatment in the presence of Hg vapor, the Tl-2212 is converted to Hg-1212 by cation exchange of Hg for Tl, using competitive processing times. A resulting coating, deposited on a $LaAlO_3$ substrate, exhibited a T_c of 124K, and excellent critical current density, J_c (Fig. 1). Here, the value of $J_c \sim 1$ MA/cm^2 at 77K in self-field corresponds to an equivalent tape current of 300 A/cm-width. While the higher T_c provides operational headroom for many applications, the performance of Hg-1212 in large magnetic fields is inferior to the less anisotropic YBCO. However, part of this problem may arise from a paucity of appropriate flux-pinning defects ordinarily formed during processing. This conjecture is supported by dramatic enhancements in both J_c and the irreversibility fields, B_{irr}, that result after columnar defects are artificially introduced parallel to the c-axis by irradiation with heavy-ions. The results in Figs. 2 and 3, show that a defect density corresponding to a matching field of 2 Tesla increases the operational parameters to practical values in that field range at liquid nitrogen temperatures. While it is impractical to create defect structures in this way for applications, these studies demonstrate the potential of enhancing properties by the introduction of defects through more appropriate processing steps.

Significance—The demonstration of large J_cs for thick (3 μm) Hg-1212 coatings on model substrates offers promise for the development of such high-current coatings on metal tapes for long-length conductors. Moreover, the processing conditions and times are amenable to large area, batch processing. The dramatic enhancements of the in-field electrical properties by heavy ion irradiation show that Hg-1212 coatings are typically formed with excessive crystalline order, and are in need of processing protocols that will introduce appropriate flux-pinning defects.

Contact: D.K. Christen, Oak Ridge National Laboratory
Phone: (423) 574-6269, Fax: (423) 574-6263, E-mail: dkc@ornl.gov

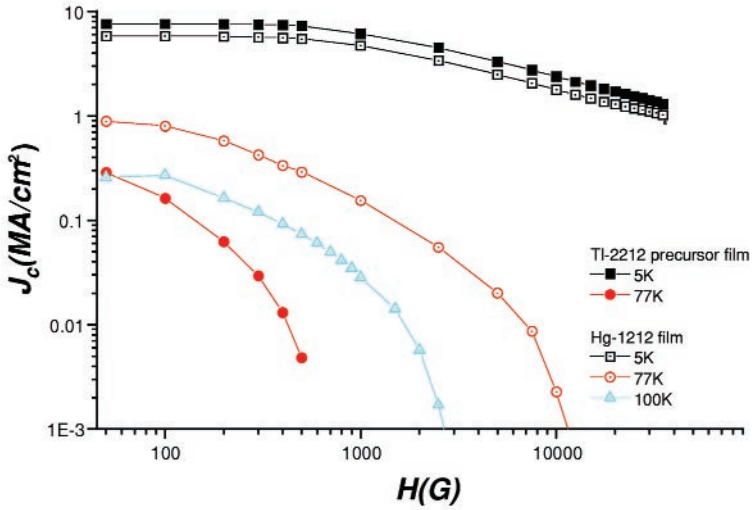

Figure 1. The magnetic field dependence of J_c for a 3μm thick epitaxial coating of Hg-1212 on a $LaAlO_3$ substrate, compared to that of the Tl-2212 precursor film used for the cation exchange process. The J_c values were deduced from magnetization hysteresis using the Bean model.

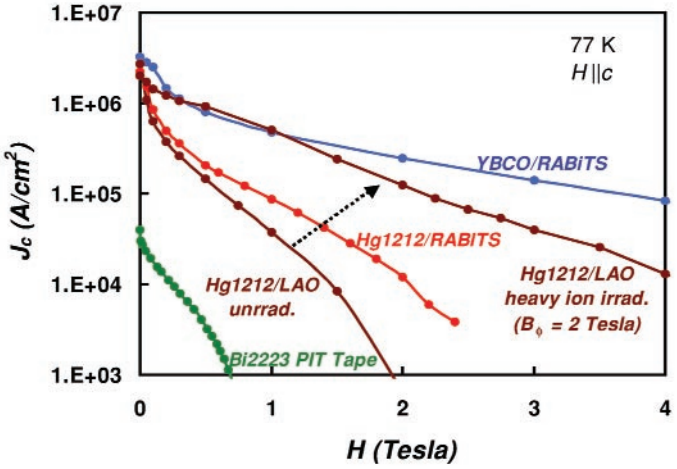

Figure 2. Comparison of transport critical current densities of various coatings. The Hg-1212 films show dramatic improvement in J_c *(H)* after irradiation with 1.2 GeV U-ions.

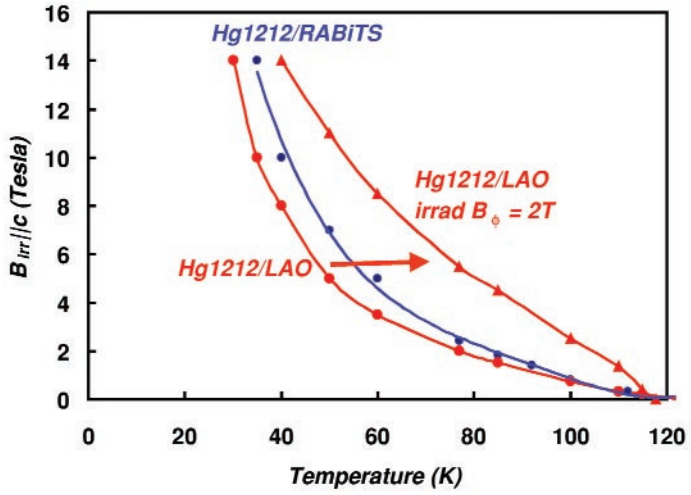

Figure 3. The irreversibility region of epitaxial Hg-1212 films is expanded by ~20K after irradiation with heavy ions.

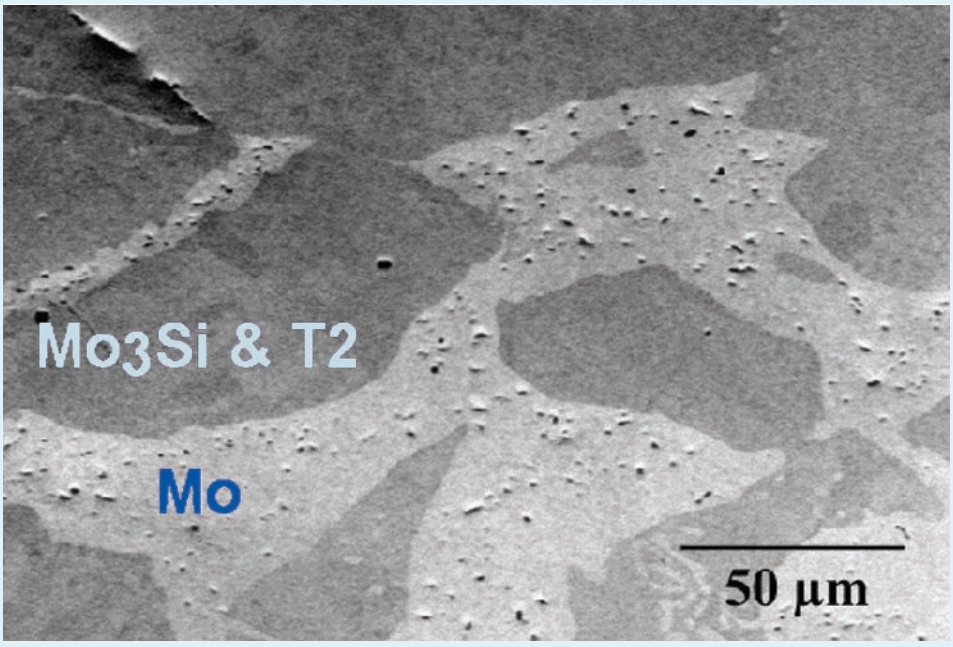

The figures on the front and back covers relate to two of the accomplishments described in this issue of *Research Briefs*. The figure on the front shows a contour plot of the stress in the vicinity of a surface crack in an oxide thin scale calculated using a finite element continuum model. Thermally-grown oxide scales provide high temperature corrosion protection for metals. The above figure shows a dispersion of Mo_3Si and Mo_5SiB_2 (T2) phases in a continuous α-Mo phase. Varying the volume fraction and ligament size of the α-Mo maxtrix allows control over the mechanical properties of the composite.

SAND2001-3474P: Prepared by the DOE Center of Excellence for the Synthesis and Processing of Advanced Materials at Sandia National Laboratories, Albuquerque, New Mexico 87185 for the Division of Materials Sciences and Engineering, Office of Basic Energy Sciences, U.S. Department of Energy. Sandia is a multiprogram laboratory operated by Sandia Corporation, a Lockheed Martin Company, for the Department of Energy under Contract No. DE-AC04-94AL85000.

Printed in August 2001